

Meson Structure in Deep Inelastic Scattering

Takayuki Shigetani, Katsuhiko Suzuki ^{*} and Hiroshi Toki [†]

Department of Physics, Tokyo Metropolitan University

Hachiohji, Tokyo 192-03, Japan

Abstract

We study the deep inelastic structure functions of mesons within the Nambu and Jona-Lasinio model. We calculate the valence quark distributions in π , K , and ρ mesons at the low energy model scale, which are evolved to the experimental momentum scale in terms of the Altarelli-Parisi equation. The resulting distribution functions show reasonable agreements with experiment. We also discuss the semi-inclusive lepton nucleon scattering process with a slow nucleon in coincidence in the final state, which reveals the off-shell structure of the pion.

^{*}e-mail address : ksuzuki@atlas.phys.metro-u.ac.jp

[†]also RIKEN, Wako, Saitama, 351, Japan

1 Introduction

The deep inelastic scattering (DIS) of hadrons is one of the most powerful tool to investigate their internal quark structure. In the last decade, the nucleon structure function has been extensively studied, and provided us with detailed information of the nucleon structure[1]. The observed scaling violations of the structure functions are consistent with the perturbative QCD predictions, though at the present QCD can not predict the structure function itself.

On the other hand, it is of great interest to clarify a connection between DIS information and the low energy quark models[2]. At the experimental large momentum scale, the virtual photon sees the hadron as a complicated object, which consists of valence quarks, sea quarks, and gluons. As the momentum scale becomes smaller, sea quarks and gluons are absorbed into valence quarks, and their degrees of freedom are substituted by the 'constituent quarks', whose dynamics is subject to the low energy QCD. If we relate the DIS data with the quark models, we can learn how the non-perturbative aspects of QCD, e.g. confinement and chiral symmetry breaking, reflect the behavior of the quark distributions at the DIS scale. Recently, such theoretical studies for the nucleon structure function are made in terms of several effective quark models, which are supposed to work at the low energy scale[3, 4, 5]. Those works are based on the assumption that the structure functions at the low energy model scale $Q^2 = Q_0^2$ are obtained by calculating the twist-2 matrix elements within the effective models. In the formalism of the operator product expansion(OPE), the n -th moment of the structure function F_2 at the scale Q^2 is expanded as,

$$\int dx x^{n-2} F_2(x, Q^2) = \sum_{\tau} C_{\tau}^n(Q^2, Q_0^2) < \mathcal{O}_{\tau}^n(Q_0^2) > \quad (1)$$

where $C_{\tau}^n(Q^2, Q_0^2)$ is the Wilson coefficients calculated by the perturbative QCD, and $< \mathcal{O}_{\tau}^n(Q_0^2) >$ is the expectation value of the local operators which are evaluated at the arbitrary scale Q_0^2 . In the Bjorken limit ($Q^2 \rightarrow \infty$), only the twist-2 ($\tau = 2$) term survives and the higher twist terms become negligible ($\sim O(1/Q^2)$). Hence, once we calculate the twist-2 operators within the quark model at the low momentum scale Q_0^2

where the phenomenological model makes sense, we can get the structure function at the experimental scale Q^2 using the QCD evolution equation. Thus, the comparison with experiment can be made.

Although the available experimental data of meson structure function is much fewer than that of nucleon, the quark distributions in mesons are also important to study the quark structure of hadrons. Comparing with the nucleon case, one may extract more directly the information of the quark-quark interaction from the structure function, since we can avoid solving the complicated three body problem as in the nucleon case. In this paper, we shall calculate the quark distributions in mesons within the Nambu and Jona-Lasinio (NJL) model[6]. In this model, the gluon degrees of freedom are assumed to be frozen into a chiral invariant effective 4-point interaction in the low energy region[7]. The NJL model demonstrates the spontaneous breakdown of chiral symmetry and the emergence of the Goldstone bosons. The generalized $SU(3)_f$ NJL model reproduces the meson properties remarkably well, in spite of the lack of confinement[8, 9]. This model is also applied to the chiral phase transition at finite temperature and density[9]. All these results indicate that the NJL model possesses the essential features of QCD. Note that the NJL model satisfies the Lorentz invariance and certain kinematics. This is an advantage of our use of the NJL model, because the quark model which does not satisfy the translational invariance, e.g. the MIT bag model, gives an incorrect behavior of the quark distributions at $x = x_B = 1$ [3, 4]. This difficulty, so called the support problem, may be removed by the momentum projection. However, some ambiguities exist in the projection methods[10].

In the recent work of present authors[11], the pion and kaon structure functions were calculated in the NJL model, and our results turned out to be consistent with experiment. In that work, however, we used an *artificial* momentum cutoff to reproduce the experimentally known behavior around $x \sim 1$. Here, we newly fix the momentum cutoff procedure to reproduce the meson properties such as masses and decay constants, and avoid the ambiguity.

We also study the semi-inclusive lepton nucleon scattering as a possible way to measure the quark distributions in mesons. Experimentally, the pion structure function has been extracted from the Drell-Yan process[12, 13]. On the other hand, the semi-inclusive processes, e.g. $p + \ell \rightarrow n + \ell' + X$, are expected to allow a new determination of the quark distributions in the pion[14, 15, 16]. In such processes, the virtual photon probes the virtual meson clouds around the nucleon, especially pion. Hence, this experiment will determine the *off-shell* pion structure function. We can make predictions for such semi-inclusive scattering in terms of the calculated pion structure function.

This paper is arranged as follows. In sec. 2, the Nambu and Jona-Lasinio model is introduced, and its model parameters are fixed to reproduce the meson properties. Sec. 3 is devoted to the calculation of the hadronic tensor of mesons. The structure functions of the pseudoscalar channel as well as the vector channel are given in the NJL model, where twist-2 contributions are calculated in the Bjorken limit. These quark distributions are evolved to the experimental high Q^2 scale with the help of the Altarelli-Parisi equation in sec. 4. We compare them with data from the Drell-Yan experiment. The semi-inclusive processes are formulated in sec. 5. The final section is devoted to summary and discussions.

2 The Nambu and Jona-Lasinio model

The Nambu and Jona-Lasinio model[6] has attracted considerable interests as a low energy effective theory of QCD. The NJL model incorporates the chiral symmetry, which is one of the most important aspects of the low energy QCD, and provides the simple picture of its spontaneous and explicit breakdown. Recently, this model was extensively studied in several subjects of hadron physics, and gave successful results[8, 9]. The generalized

$SU(3)_f$ NJL model lagrangian is given by,

$$\begin{aligned}
\mathcal{L}_{NJL} &= \mathcal{L}_o + \mathcal{L}_4 \\
\mathcal{L}_o &= \bar{\psi}(i\gamma^\mu\partial_\mu - m)\psi \\
\mathcal{L}_4 &= G_S[(\bar{\psi}t_a\psi)^2 + (\bar{\psi}t_a i\gamma^5\psi)^2] \\
&\quad - G_V[(\bar{\psi}t_a\gamma_\mu\psi)^2 + (\bar{\psi}t_a\gamma_\mu\gamma^5\psi)^2] .
\end{aligned} \tag{2}$$

Here, ψ denotes the quark field with the current mass m . t_i are the $SU(3)$ flavor matrices, normalized as $tr(t_i t_j) = \delta_{ij}/2$, and G_S , G_V the coupling constants.

Using (2), one gets the Dyson equation for the quark propagator in the Hartree approximation (Fig.1 (a));

$$M = m - G_S \langle \bar{\psi}\psi \rangle , \tag{3}$$

where M is the dynamically generated constituent quark mass. The quark condensate $\langle \bar{\psi}\psi \rangle$ is expressed as,

$$\langle \bar{\psi}\psi \rangle = -i4N_c \int \frac{d^4p}{(2\pi)^4} \frac{M}{p^2 - M^2} , \tag{4}$$

where N_c is the number of colors. If the coupling constant G_S is larger than a critical value, the quark condensate and the constituent mass have non-zero values, which means spontaneous breakdown of the chiral symmetry.

The meson properties are obtained by solving the Bethe-Salpeter (BS) equation, illustrated in Fig.1 (b). The inhomogeneous BS equation for $q\bar{q}$ T-matrix is written symbolically as,

$$\mathcal{T} = \mathcal{K} + \mathcal{K}\mathcal{J}\mathcal{T} , \tag{5}$$

where \mathcal{T} is the T-matrix, \mathcal{K} is the interaction kernel obtained from (2), and \mathcal{J} the loop integral of a given channel. \mathcal{K} is decomposed into the various products of the gamma,

flavor and color matrices.(See ref.[8] for detail.) The loop integral \mathcal{J} is defined by,

$$\mathcal{J}_{ij}(q, M_1, M_2) = i \int \frac{d^4 k}{(2\pi)^4} \text{tr}[S(k + \frac{1}{2}q, M_1)\Gamma_i S(k - \frac{1}{2}q, M_2)\Gamma_j] , \quad (6)$$

where $S_F(k, M)$ is the quark propagator.

$$S_F(k, M) = \frac{1}{\not{k} - M}$$

The quark propagator contains the constituent mass obtained by solving the gap equation (3). The meson mass is determined as a pole of T-matrix at $q^2 = m_{meson}^2$. The quark-antiquark T-matrix (5) is rewritten as,

$$\begin{aligned} \mathcal{T}(q) &= \mathcal{K} + \mathcal{K}\mathcal{J}\mathcal{T} \\ &= \frac{\mathcal{K}}{1 - \mathcal{J}\mathcal{K}} \\ &\sim g_{mqq}\Gamma_i \frac{1}{q^2 - m_{meson}^2} \Gamma_j g_{mqq} \quad \text{at} \quad q^2 \sim m_{meson}^2 . \end{aligned} \quad (7)$$

Here, g_{mqq} is the meson-quark-quark coupling constant. The integrals in (3) and (6) diverge due to the non-renormalizability of the NJL model. Thus, we introduce the Fermi-distribution type momentum cutoff function in these integrals;

$$\int d^4 k \rightarrow i \int d^4 k_E \frac{1}{1 + \exp[(k_E^2 - \Lambda^2)/a]} . \quad (8)$$

Here, k_E^2 is the Euclidean four momentum square, and Λ is identified with the typical scale of the chiral symmetry breaking $\sim 1\text{GeV}$. We use $a \sim 0.1\text{GeV}^2$ to reproduce the meson properties. This form of the regularization function is consistent with the usual Euclidean sharp cutoff scheme[8]. One may understand the physical implication of the cutoff procedure as an approximate realization of "Asymptotic Freedom" in the NJL model, i.e. the interaction between two quarks with the relative momentum larger than Λ is turned off, and two particles are free in such a high momentum region. Hence, the structure functions obtained in the NJL model exhibit the exact Bjorken scaling in the deep inelastic limit[17].

Solving the BS equation (5), we can obtain the meson masses, and the decay constants. We take the current mass of the up and down quarks $m_{u,d} = 5.5 MeV$ as a semi-empirical value. The remaining parameters are fixed by the pseudoscalar meson properties. The parameters and the resulting physical properties are tabulated in Table 1. Using this model, we shall describe the deep inelastic structure of mesons.

3 Calculation of the Hadronic Tensor

We evaluate the structure functions of mesons in the NJL model, as done in ref.[11]. The calculated distribution gives a boundary condition for the QCD perturbation at the model scale. The hadronic tensor $W_{\mu\nu}$ is written by the structure functions $F_1(x)$ and $F_2(x)$ in the scaling limit;

$$W_{\mu\nu} = - \left(g_{\mu\nu} - \frac{q_\mu q_\nu}{q^2} \right) F_1(x) + \frac{1}{m_{ps}\nu} \left(p_\mu - \frac{p \cdot q}{q^2} q_\mu \right) \left(p_\nu - \frac{p \cdot q}{q^2} q_\nu \right) F_2(x) \quad (9)$$

where

$$F_2(x) = x \sum_i e_i^2 [q_i(x) + \bar{q}_i(x)] , \quad F_1(x) = \frac{1}{2x} F_2(x)$$

$q_i(x)$ and $\bar{q}_i(x)$ are the momentum distributions of i-flavor quark and antiquark. The hadronic tensor is related to the forward scattering amplitude $T_{\mu\nu}$ through the optical theorem[1].

$$W_{\mu\nu} = \frac{1}{2\pi} Im T_{\mu\nu} . \quad (10)$$

Thus, we calculate $T_{\mu\nu}$ in the NJL model to get the structure functions.

We first consider the pseudoscalar meson case. We compute the forward scattering amplitude in the impulse approximation, which is illustrated in Fig.2 ("handbag diagrams").

Here, p is the momentum of a target meson, and q the momentum delivered by the virtual photon. We expand the matrix elements of Fig.2 as a series of $1/Q^2$. The leading $O((1/Q^2)^0)$ term of the "handbag diagram" coincides with the twist-2 contribution of the OPE in the Bjorken limit[18]. Thus, this diagram is enough for our purpose. We note that, though leading terms do not depend on Q^2 explicitly, they receive the logarithmic QCD radiative corrections, which are incorporated by the Altarelli-Parisi equation. The matrix elements of Fig.2 are given by,

$$T_{\mu\nu} = i \int \frac{d^4k}{(2\pi)^4} \text{Tr}[\gamma_\mu Q \frac{1}{\not{k}} \gamma_\nu Q T_-] + (T_+ \text{ term}), \quad (11)$$

where

$$T_- = S_F(k - q, M_1) g_{pqq} \tau_+ i \gamma_5 S_F(k - q - p, M_2) g_{pqq} \tau_- i \gamma_5 S_F(k - q, M_1) \quad (12)$$

T_- represents the contribution with an antiquark being a spectator. T_+ also has a similar expression, where a quark is a spectator. Here, g_{pqq} is the coupling constant among two quarks and the pseudoscalar meson obtained from (7), Q the charge operator, and $\tau_\pm = (\tau_1 \pm i \tau_2)/\sqrt{2}$. M_1 is the constituent mass of the struck quark, and M_2 the mass of the spectator antiquark, which are solutions of the gap equation (3) due to the dynamical chiral symmetry breaking. In the case of pion, we set $M_1 = M_2 = M_{u(d)}$. For K^+ meson, $M_1 = M_u$ and $M_2 = M_S$.

We shall carry out the integration of (12) in the Bjorken limit[19, 11];

$$Q^2 = -q^2 \rightarrow \infty, \quad \nu = \frac{p \cdot q}{m_{ps}} \rightarrow \infty, \quad x = \frac{Q^2}{2m_{ps}\nu} : \text{fixed.}$$

Here, x is the so-called Bjorken x , and m_{ps} the pseudoscalar meson mass. We introduce the Sudakov variables;

$$k_\mu = zp_\mu + yq_\mu + \kappa_\mu, \quad (13)$$

where κ_μ satisfies $k \cdot p = k \cdot q = 0$. Thus, κ_μ is spacelike ($\kappa^2 < 0$) and is effectively

two dimensional. Calculating the traces and neglecting irrelevant terms in the Bjorken limit[19], we obtain,

$$T_{\mu\nu}^{(-)} = \frac{8}{9} \frac{i}{(2\pi)^4} N_c g_{pqq}^2 \int dz d\bar{y} d^2\kappa [t_1(\mu^2, s) + z t_2(\mu^2, s)] \frac{1}{z-x} \\ \times \left[-g_{\mu\nu} + \frac{2z}{m_{ps}\nu} p_\mu p_\nu + \frac{1}{m_{ps}\nu} (p_\mu q_\nu + p_\nu q_\mu) \right], \quad (14)$$

where

$$t_1(\mu^2, s) = -\frac{1}{(\mu^2 - M_1^2 + i\varepsilon)^2} \frac{1}{s - M_2^2 + i\varepsilon} (\mu^2 - M_1^2) \\ t_2(\mu^2, s) = -\frac{1}{(\mu^2 - M_1^2 + i\varepsilon)^2} \frac{1}{s - M_2^2 + i\varepsilon} (s + M_1^2 - 2M_1 M_2 - p^2),$$

and

$$\mu^2 = (k - q)^2 = z\bar{y} + \kappa^2 \\ s = (k - q - p)^2 = (z - 1)(\bar{y} - p^2) + \kappa^2.$$

Here, we change the variable $\bar{y} = 2m_{ps}\nu(y - 1) + zp^2$ [19], and μ^2 and s are the invariant masses of the struck quark and spectator. Performing the z -integral in (14), we find[19, 18],

$$T_{\mu\nu} = \frac{8}{9} \frac{1}{(2\pi)^3} N_c g_{pqq}^2 \int d\bar{y} d^2\kappa [t_1(\mu^2, s) + z t_2(\mu^2, s)] \\ \times \left[-g_{\mu\nu} + \frac{2z}{m_{ps}\nu} p_\mu p_\nu + \frac{1}{m_{ps}\nu} (p_\mu q_\nu + p_\nu q_\mu) \right]. \quad (15)$$

It is easily seen from (15) that the calculated structure functions exhibit the Bjorken scaling[17]. Consider now the \bar{y} -integral in the complex \bar{y} -plane. The s -propagator has a pole at $\bar{y} = (\kappa^2 - M_2^2)/(1 - x) + p^2 + i\varepsilon/(1 - x)$, and the μ -propagator has a double pole at $\bar{y} = (M_1^2 - \kappa^2)/x - i\varepsilon/x$. For $x > 1$ or $x < 0$, all these singularities occur on the same side of the real \bar{y} -axis, and (15) gives a zero result[19, 18]. However, if $0 \leq x \leq 1$, the integration over \bar{y} no longer vanishes. Integrating (15) by \bar{y} and taking the imaginary part, we get the quark distribution by use of the optical theorem (10). We change the

integral variable κ^2 to μ^2 , and find the following expression for the quark distribution function.

$$q(x) \propto -g_{pqq}^2 \int_{-\infty}^0 d\mu^2 \left[\frac{1}{\mu^2 - M_1^2} - x \frac{2M_1 M_2 - (M_1^2 + M_2^2) + p^2}{(\mu^2 - M_1^2)^2} \right] \times \theta(p^2 x(1-x) - xM_2^2 - (1-x)\mu^2) \quad (16)$$

Here, θ is the usual step function which arises from the spacelike condition of κ . We identify (16) as the valence quark distribution of the pseudoscalar meson $q_{val}(x)$. In the case of on-shell pseudoscalar meson, we use $p^2 = m_{ps}^2$. We use the Euclidean variable $\mu_E^2 = -\mu^2$ for the integration of (16) with the relative momentum cutoff (8). Note that the resulting distribution shows a correct behavior $q(x) \rightarrow 0$ as $x \rightarrow 1$, since the lower limit of the integral $\mu_{E\min}^2 (= -\mu_{\max}^2) = \frac{x}{1-x} M_2^2 - xp^2 \rightarrow \infty$ as $x \rightarrow 1$ and thus the integral vanishes[17]. We also note that the contribution of the second term of (16) to the distribution function is small. This smallness is due to the spontaneous breakdown of the chiral symmetry. In fact, the second term disappears in the chiral limit; $m_u = m_d = m_s = 0$. This form ensures the behavior $xq_{val}(x) \propto x$ at small x . If the chiral symmetry were not spontaneously broken, the second term would be as large as the first term and the pionic quark distribution would behave $xq(x)_{val} \propto x^2$ around small x .

We also apply the same procedure to the vector meson, though the NJL model does not work well in the vector channel[8]. Since the vector mesons, e.g. ρ meson, may be weakly coupled quark-antiquark states, the confinement of quarks is essential for the description of them. Hence, it is not adequate to use the NJL model for the vector mesons due to the absence of confinement in this model. However, such an attempt is still worth mentioning for an intuitive understanding of the relation between the structure function and the quark interaction.

The hadronic tensor of the spin-1 vector meson is defined as,

$$W_{\mu\nu}^{\alpha\beta} = \left[-\left(g_{\mu\nu} - \frac{q_\mu q_\nu}{q^2} \right) F_1(x) \right]$$

$$+ \frac{1}{m_V \nu} (p_\mu - \frac{p \cdot q}{q^2} q_\mu) (p_\nu - \frac{p \cdot q}{q^2} q_\nu) F_2(x)] (-g^{\alpha\beta} + \frac{p^\alpha p^\beta}{p^2}) \quad (17)$$

where α, β is the polarization of the vector meson, and m_V the vector meson mass. This form guarantees the current conservation, i.e. $p_\alpha W_{\mu\nu}^{\alpha\beta} = p_\beta W_{\mu\nu}^{\alpha\beta} = 0$. Contracting with the meson polarization vector $\epsilon_\alpha, \epsilon_\beta$ and summing over the helicity λ , we find the expression of the unpolarized structure function;

$$\begin{aligned} W_{\mu\nu} &= \sum_\lambda \varepsilon_\alpha(\lambda, p)^* \varepsilon_\beta(\lambda, p) W_{\mu\nu}^{\alpha\beta} \\ &= (-g^{\alpha\beta} + \frac{p^\alpha p^\beta}{p^2}) W_{\mu\nu}^{\alpha\beta} \\ &= 3[-(g_{\mu\nu} - \frac{q_\mu q_\nu}{q^2}) F_1(x) \\ &\quad + \frac{1}{m_V \nu} (p_\mu - \frac{p \cdot q}{q^2} q_\mu) (p_\nu - \frac{p \cdot q}{q^2} q_\nu) F_2(x)] \end{aligned} \quad (18)$$

Corresponding to (12), $T_-^{\alpha\beta}$ in the vector channel is given by,

$$T_-^{\alpha\beta} = S_F(k - q, M) g_{Vqq} \tau_+ \gamma^\alpha S_F(k - q - p, M) g_{Vqq} \tau_- \gamma^\beta S_F(k - q, M). \quad (19)$$

Here, we omit the mass difference of the struck and spectator quarks for simplicity. After some trivial algebras, we obtain the quark distribution in the vector meson.

$$\begin{aligned} q(x) \propto & -g_{Vqq}^2 \int d\mu^2 [\frac{1-x}{p^2} - \frac{2}{\mu^2 - M^2} + \frac{2x(p^2 + 2M^2)}{(\mu^2 - M^2)^2}] \\ & \times \theta(p^2 x(1-x) - xM^2 - (1-x)\mu^2) \end{aligned} \quad (20)$$

Here, $p^2 = m_V^2$. We remark that the expression for the quark distribution in the vector meson is quite different from that of the pseudoscalar meson. In contrast to the pion case, the quark distribution function of the rho meson behaves $xq(x)_{val} \propto x^2$ at the small x , due to the large contribution of the third term in (20).

Unfortunately, it was shown that the mass of ρ meson is more than two times the constituent quark mass, and it should decay into two quark states, within the standard parameters of the NJL model[8]. Thus, we use a larger value for the constituent quark mass ($400MeV$) and G_V without changing other values to obtain a 'bound state' for ρ meson.

4 Numerical Results

In this section, we will show numerical results for quark distribution functions with the use of the parameters in Table 1. We first show in Fig.3 the quark distribution in the pion (16) at the low energy model scale. The peak of the resulting distribution appears at $x \sim 0.6$, which indicates asymmetric momentum distributions in the pion; the struck quark carries a larger part of the pion momentum. This is due to large binding energy of the valence quark in the pion. Such a behavior is also suggested by the QCD sum rule calculation[20]. This result is a consequence of the highly non-perturbative structure of the pion

The valence quark distribution of kaon is also interesting. We can extract the effects of the explicit $SU(3)$ flavor symmetry breaking from the quark distribution of kaon. The u- and s-quark distributions of the kaon at the low momentum scale are presented in Fig.4. The heavy strange quark carries a larger fraction of kaon momentum than the light up(down) quark, as expected.

We note that this low energy scale structure function has no physical meaning at this scale, since "real" structure function at the low energy scale receives non-negligible contributions from all twist operators. The calculated results in Fig.3 and Fig.4 play roles of only the boundary condition of the structure function for the Q^2 evolution.

We take the low energy hadronic scale at $Q_0^2 = (0.5GeV)^2$, which is used in ref. [21]. At this scale, the running coupling constant is still small; $\alpha_s(Q_0^2)/\pi \sim 0.3$. Indeed, the

inclusion of the second order QCD corrections gives a small change for the Q^2 evolution from our result within 10%[21].

We may understand intuitively the physical meaning of this scale Q_0^2 as compared to the valence quark core radius of pion $\langle r^2 \rangle_{core}$, as noted by Brown *et al.*[22]. In their analysis of the pion electromagnetic form factor, the pion consists of the valence quark core part, where a valence quark and an antiquark move in the small region, and the sea quark cloud part which is understood as the old vector meson dominance. Their value is consistent to our low energy scale;

$$\langle r^2 \rangle_{core} \sim (0.35 fm)^2 \sim 1/(0.5 GeV)^2 .$$

We use the first order Altarelli-Parisi equation[23] for the Q^2 evolution of valence distributions with $\Lambda_{QCD} = 250 MeV$ to compare our results with experiment.

$$\frac{dV(x, Q^2)}{d(\log Q^2)} = \frac{\alpha_s(Q^2)}{2\pi} \int_x^1 dx P_{qq}(x/y) V(y, Q^2)$$

Here, $V(x, Q^2)$ is the valence quark distribution, and P_{qq} the splitting function[23].

We show in Fig.5 the pionic quark distribution at $Q^2 = 20 GeV^2$ by the solid curve with experimental data (the dashed curve) extracted from the Drell-Yan process[24]. We find a reasonable agreement with experiment. The second moment of the valence quark, which is identified with a momentum fraction carried by the valence quark, turns out to be,

$$\langle xu \rangle_{\pi} = 0.22 \quad \text{at} \quad Q^2 = 20 GeV^2 ,$$

where $\langle xq \rangle = \int_0^1 dx xq(x)$. This value is remarkably consistent with experimental data 0.21[24]. However, the calculated distribution function is almost zero at $x \sim 1$, and different from the experimental fit[24] or the counting rule prediction[1]. This shortcoming comes from the cutoff procedure of the model. Around $x \sim 1$, the struck quark has a very large momentum $> 1 GeV$, and the quarks with so large momenta are excluded in the NJL model by the cutoff. At the moment, such a high momentum quark can not

exist in the hadron wave function within the low energy quark model, and we ought to develop a model to include the high momentum correlations consistently with the low energy theory.

If we vary the low energy scale Q_0^2 within 20%, the change of the quark distribution is rather small ($\sim 10\%$). As an example, we plot in Fig.6 the result in which we use $Q_0^2 = 0.7\text{GeV}^2 \sim \Lambda_{NJLcut}^2$. The peak position of the calculated distribution is $x \sim 0.5$, which disagrees with experiment.

We compare the pion structure function $F_\pi(x)$ with experiment in Fig.7. Here, we do not take into consideration the sea quark distributions, since we do not evaluate the sea quark diagrams at the model scale. It shows a good agreements for $x > 0.3$. In the low x region, the structure function is dominated by the sea quark distributions. As for the sea quarks, we can calculate their distribution functions at the model scale as higher order loop corrections in the NJL model[25]. We will discuss this point later.

The quark distributions in kaon are also evolved to the experimental scale in Fig.8. The resulting distributions show a similar flavor dependence with the previous results obtained by the Regge theory [26, 27]. The corresponding second moments of the valence quarks are given by,

$$\langle xu \rangle_K = 0.20, \quad \langle xs \rangle_K = 0.24 \quad \text{at} \quad Q^2 = 20\text{GeV}^2.$$

This result indicates that the heavy strange quark has a larger momentum in kaon than the light u(d) quark. These values are to be compared with the pion case; $\langle xu \rangle_\pi = 0.22$. The total momentum carried by the valence quarks in the kaon is $\langle xu \rangle_K + \langle xs \rangle_K = 0.44$, and is almost the same as that in the pion $2\langle xu \rangle_\pi = 0.43$. Similar results are obtained by the recent QCD sum rule calculation[28].

We also show in Fig.9 the ratio of kaon to pion valence u-quark distributions u_K/u_π at $Q^2 = 20\text{GeV}^2$. The experimental values are taken from the Drell-Yan experiment[13], and the analysis of the large transverse momentum π_0 production processes[29]. The result is consistent with available experiments. Note that this ratio is sensitive to the mass difference of the constituent quark masses in our model. In fact, if we change the constituent

strange quark mass, the resulting ratio becomes quite different from experiment. We plot two cases ($M_s = M_u$ and $M_s = 2M_u$) in Fig.9 for comparison.

Finally, we show in Fig.10 the quark distribution in the rho meson at the model scale. This behavior is extremely different from the result of the pion. The resulting distribution shows a sharp peak at $x \sim 0.5$ due to the weak correlation in the vector channel, and resembles with the result of the non-relativistic static limit $q(x) \sim \delta(x - 1/2)$. Similar behavior is obtained in ref. [30]. Although the NJL model in the vector channel has some difficulties[8], the essential feature of this distribution is expected to be model independent.

5 Semi-inclusive lepton nucleon scattering

Since a direct experiment of the lepton-pion deep inelastic scattering is beyond the present experimental abilities, the information of the pion structure function can be extracted from only the μ -on pair production process, as first suggested by Drell and Yan[12]. Several authors considered an alternative approach to determine the pionic quark distributions[14, 15, 16]. In the semi-inclusive lepton nucleon scattering illustrated in Fig.11, virtual meson clouds mainly contribute to this process in the case of a slow nucleon in the final state. This contribution is expected to be dominated by the one-pion exchange from the study of the inclusive process $p + p \rightarrow n + X$, in which the kinematical condition is similar with the semi-inclusive process mentioned above; the proton beam carries the incident energy $\sim 10GeV$ and the momentum of the final state neutron is $\sim 500MeV$ [31].

It is also important to study such virtual pion processes in view of the recent experimental observation, i.e. 'the violation of the Gottfried sum rule'[32]. The pion clouds make substantial contributions to the violation of the flavor symmetry in the nucleon sea [33, 34]. In such a virtual pion lepton scattering, the current sees the off-shell structure

of the pion. Here, we reexamine these processes by taking into account the off mass shell dependence of the pion structure function, which is neglected in the previous works.

We consider the following process; (Similar expression can be developed for the neutrino beam.)

$$e + p \rightarrow e' + n + X.$$

The calculations are performed at the target rest frame with the z-axis fixed by the current. Following the work of Lusignoli *et al.*, we define kinematical variables shown in Fig.11[15].

$$\begin{aligned} k &= E_L(1, \sin \psi, 0, \cos \psi) && \text{for the incident electron} \\ k' &= E'_L(1, \sin(\psi + \theta_L), 0, \cos(\psi + \theta_L)) && \text{for the outgoing electron} \\ P_i &= M(1, 0, 0, 0) && \text{for the target nucleon} \\ P_f &= (E, p \sin \alpha \cos \beta, p \sin \alpha \sin \beta, p \cos \alpha) && \text{for the outgoing nucleon} \end{aligned} \quad (21)$$

Here, M is the nucleon mass, and θ_L the angle between the electron momenta, and $\tan \psi = E'_L \sin \theta_L / (E_L - E'_L \cos \theta_L)$, which is chosen to provide $q = k' - k$ to have only the z-component. p is the three momentum of the final state neutron. The definition of the Bjorken variables are as follows;

$$\nu = q \cdot P_i / M, \quad Q^2 = -q^2 = 4E_L E'_L \sin^2 \frac{1}{2} \theta_L, \quad x = Q^2 / 2M\nu. \quad (22)$$

For the pion, we need to define its momentum and a quark momentum fraction in the pion.

$$P_\pi = P_i - P_f, \quad t \equiv P_\pi^2 = 2M(M - E), \quad x_\pi = Q^2 / 2q \cdot P_\pi \quad (23)$$

It is easily shown that x_π is related with the Bjorken x as;

$$\frac{x}{x_\pi} = \frac{q \cdot P_\pi}{q \cdot P_i} = 1 - \frac{E}{M} + \frac{\sqrt{\nu^2 + Q^2}}{\nu} \frac{p}{M} \cos \alpha. \quad (24)$$

The requirement of the kinematics implies the following conditions with $\nu \rightarrow \infty$,

$$x \leq x_{\max} \sim 1 - (E - p)/M \leq 1, \quad \cos \alpha \geq \frac{E}{p} - \frac{M}{p}(1 - x). \quad (25)$$

The total (unobserved) missing mass M_X of this process is given by,

$$M_X^2 = (q + P_\pi)^2 = Q^2 \left(\frac{1}{x_\pi} - 1 \right) + t. \quad (26)$$

The condition of the deep inelastic scattering also requires the sufficiently large missing mass. In the present study, we assume that M_X is larger than 2GeV ; $M_{X\min} = 2\text{GeV}$. Thus, the variable x_π is constrained by the above conditions as;

$$x \leq x/x_{\max} \leq x_\pi \leq \frac{Q^2}{Q^2 - t + M_{X\min}^2} \leq 1. \quad (27)$$

The cross section of the electron-proton process is calculated as[15],

$$\begin{aligned} \frac{d\sigma}{dE'_L d\cos\theta_L d^3p} &= \frac{4\alpha^2}{\pi Q^4} \frac{g_{\pi NN}^2}{4\pi} \frac{E_L'^2}{ME} \frac{-t}{(t - m_\pi^2)^2} \\ &\times \left\{ 2 \sin^2 \frac{1}{2} \theta_L F_1^\pi(x_\pi, Q^2, t) \right. \\ &\left. + \left[\frac{(k \cdot P_\pi)(k' \cdot P_\pi)}{E_L E_L'} - t \sin^2 \frac{1}{2} \theta_L \right] \frac{F_2^\pi(x_\pi, Q^2, t)}{q \cdot P_\pi} \right\}, \end{aligned} \quad (28)$$

where

$$F_1^\pi(x_\pi, Q^2, t) = \frac{1}{2x_\pi} F_2^\pi(x_\pi, Q^2, t) \quad (29)$$

is the pion structure functions. m_π is the pion mass, and $g_{\pi NN} = 13.5$ the pion-nucleon coupling constant.

For the pion exchange mechanism, we examine the elementary pion with the dipole πNN form factor and the Reggeized pion. In the former case, the pion-nucleon coupling

becomes,

$$g_{\pi NN} \Rightarrow g_{\pi NN} \frac{(1 - m_\pi^2/\Lambda^2)^2}{(1 - t/\Lambda^2)^2} \quad (30)$$

where $\Lambda = 1\text{GeV}$ is the momentum cutoff of the πNN interaction. On the other hand, in the latter case, we replace the pion propagator square with the triple Regge formula[15].

$$\frac{1}{(t - m_\pi^2)^2} \Rightarrow \pi^2 \alpha'^2 \frac{1 + \cos[\pi\alpha_\pi(t)]}{2 \sin^2[\pi\alpha_\pi(t)]} e^{b(t - m_\pi^2)} \left[\frac{1/x_\pi - 1 - t/q^2}{1/x - 1 - M^2/q^2} \right]^{-2\alpha_\pi(t)} \quad (31)$$

Here, $\alpha_\pi(t) = \alpha'(t - m_\pi^2)$ with $\alpha' = 1\text{GeV}^{-2}$. Exponential damping factor b is chosen phenomenologically to reproduce the data of $p + p \rightarrow n + X$ scattering; $b = 0.56\text{GeV}^{-2}$.

We first show in Fig.12 the off-shell t -dependence of the pion structure function evolved to $Q^2 = 20\text{GeV}^2$, using (16), where $p^2 = t$ and $g_{\pi qq}(t)$. Here, $g_{\pi qq}(t)$ is almost unchanged from the on-shell case. This effect is neglected in the previous works[15]. As the pion momentum t increases, the peak position of the quark distribution moves toward the small x region, and the distribution function shows a substantial reduction for $x > 0.4$. Around $x \sim 0.5$, the absolute value of the distribution function at $t = -0.5\text{GeV}^2$ is almost half of that for the on-shell case. This decrease is crucial to understand the following results.

Using (28) with (30) or (31), we obtain the cross section with the incident electron energy $E_L = 30\text{GeV}$. Here, we use the distribution functions at $Q^2 = 20\text{GeV}^2$ shown in Fig.12 for simplicity, since the change of distributions due to the Q^2 evolution is rather small ($\leq 20\%$) in the momentum region above $Q^2 = 5\text{GeV}^2$, which is about the same size as the experimental uncertainty of the pion structure function[34].

For comparison, we also present the results with other plausible forms of the pion structure function; the experimental fit of Sutton *et al.*[24], and the parameterization of Glück *et al.*[21]. These are chosen to reproduce the on-shell data of the pionic distribution, that is, they do not depend on the pion momentum. In each figure, we show our calculation by the solid curve. The results with the distribution functions of Sutton *et al.* and Glück *et al.* are depicted by the dashed and dotted curves, respectively.

Concerning the sea quark distribution, we do not calculate it at the model scale, and thus we can not estimate its contribution. Experimental determination also contains a large uncertainty[24]. Hence, we simply use the parameterization of Glück *et al.*[21] for the sea quark distributions in all the cases. The sea quark contribution to the cross section is negligible for $x > 0.3$.

We show in Fig.13 ($d\sigma/dp$) with p being the three momentum of the neutron in the final state. We utilize the triple Regge formula (31) in Fig.13 (a), and the dipole vertex (30) in Fig.13 (b). The results depend on the type of the πNN vertex, especially $p > 0.3GeV$, whereas they are almost independent of the choice of the structure function, i.e. the off-shell effect is not evident. Thus, we can get the most suitable form of the πNN exchange process from these figures by comparing with the forthcoming experimental data.

We next discuss the x dependence of the cross section ($d\sigma/dx$) shown in Fig.14 (a) and (b). For $x > 0.3$, the resulting cross section shows a clear difference between ours and others. The result with the off-shell structure function is much smaller than that with the experimental fit for $x > 0.3$. Note that the sea quark contribution is very small for $x > 0.3$. Hence, this difference is caused purely by the change of the valence quark distribution function. It is understood as a convolution effect. Roughly speaking, the cross section at x is expressed as an integral of the pion structure function $F_\pi(x_\pi)$. Because of (27), this integration over x_π is essentially carried out from x to 1, namely, the partons with the momentum fraction $x_\pi \geq x$ in the pion do contribute to the cross section at x . Thus, the cross section is more sensitive to the change of the large x_π behavior of the distribution function. We recall that the reduction of the calculated off-shell distribution function from the on-shell one becomes large at the large x region shown in Fig.12. Therefore, as x increases, the difference of the two cross sections becomes considerably large.

Unfortunately, all of this decrease is not originated from the off-shell effect. To see this point, we also present the result by the dash-dotted curve in Fig.14, using the calculated pion structure function with no off-shell dependence, i.e. we neglect the t -dependence of the distribution function and fix $t = m_\pi^2 = (140MeV)^2$. It gives slightly smaller cross

section than those of Sutton *et al.* and Glück *et al.* for $x > 0.3$. This reduction comes from the discrepancy between our calculation and the empirical distribution function for the on-shell pion, already shown in Fig.5. Because our quark distribution is different from the empirical one at $x \sim 1$, this disagreement reduces the cross section. However, our two results, t -dependent case and $t = m_\pi^2$ fixed case, also show a clear difference in Fig.14. This reduction of the cross section is due to the real off-shell effect, as discussed above.

6 Summary and Discussions

In this paper, we have studied the deep inelastic structure function of mesons using the Nambu and Jona-Lasinio model as a low energy effective model of QCD. The calculations of the leading twist operator are performed at the low energy model scale Q_0^2 , and the resulting distributions are evolved to the experimental large momentum scale in terms of the Altarelli-Parisi equation. Although next to leading order contributions of the QCD evolution are small[21], it is very difficult to estimate uncertainties for the use of the QCD perturbation below 1GeV .

Our results are in reasonable agreements with experimental data, except for the large x region. In this region, the struck quark carries a large momentum $> 1\text{GeV}$, and the NJL model is not designed for the momentum $p^2 > \Lambda^2 \sim 1\text{GeV}^2$. Generally, the phenomenological quark wave functions, e.g. Isgur-Karl model(Harmonic oscillator type) or the MIT bag model, do not include such high momentum components. We should improve the behavior of the structure function at the large x , by taking into account the quark correlation in the high momentum region. Higher twist contributions are also expected to change the shape of the distribution function at the large x . Indeed, experimental analysis of the scaling violation indicates that higher twists give non-negligible contributions to the nucleon structure functions in the large x region. If the pion is a collective $q\bar{q}$ state, twist-4 contributions may be larger than those of the nucleon.

The extraction of the flavor symmetry breaking effects in DIS is also important. By studying the differences between quark distributions of various flavors, we obtain the information about the flavor dependence of their internal wave functions in hadrons, e.g. the nucleon structure function gives the spin-flavor structure of the valence quarks for the u- and d-quarks[35]. The kaon structure function provides the valuable data on the strange sector. As we have discussed for the kaon, the valence strange quark may carry larger momentum fraction than the up or down quark in the kaon. Comparing the u-quark distribution in the kaon $u_K(x)$ with that in the pion $u_\pi(x)$, the NJL model calculation indicates the dominance of $u_\pi(x)$ at the large x , and is consistent with the available data. This is due to the strong quark correlation in the pion, namely, the binding energy of the u-quark in the pion is larger than that in the kaon.

The investigation of the semi-inclusive lepton nucleon scattering is very interesting as an alternative method to extract the virtual meson contributions to the nucleon structure. From them, we can obtain the off-shell dependence of the quark distribution function in the virtual pion. It also helps deeper understandings of the $SU(2)$ flavor symmetry breaking in the nucleon sea. The calculated distribution function shows rather large momentum dependence. The pion structure function decreases as the spacelike momentum of the pion t becomes large, particularly for $x > 0.4$. We have computed the cross section with the use of the off-shell pion structure function and the on-shell one, and found the cross section of the off-shell t -dependent case is much smaller than the $t = m_\pi^2$ fixed case for $x > 0.3$. In order to compare our calculations with the forthcoming experiment, we ought to study this process more rigorously with the improvement of the large x behavior of the distribution function, e.g. estimation of contributions from other mesons and nucleon resonances, or inclusion of the interference of the π and η meson[16]. Such a study is under investigation[36].

Here, we comment on the sea quark distributions in the NJL model. The lowest order diagram for the sea quark distributions is shown in Fig.15 (a), corresponding to Fig.1 (a), which is very important for the calculation of the quark self-energy and hence

the spontaneous chiral symmetry breaking. As discussed by Bernard *et al.*[17], however, this sea quark diagram does not contribute to the structure function in the NJL model, since it has no imaginary part. In order to get the 'meaningful' sea quark distribution in the model, we must calculate next to leading order diagram shown in Fig.15 (b), which are usually neglected within the Hartree approximation. This inconsistency of the approximation is a defect of the NJL model. It can be shown that the contribution of the next to leading order diagram to the quark self-energy is about 10% of the total constituent mass. Therefore, the sea quark distribution is expected to share the momentum fraction of the same magnitude in the pion at the low energy model scale[37].

Our approach in terms of the NJL model achieves qualitative agreements with the existing experimental data. The calculated quark distributions reflect the low energy quark dynamics of the model, i.e. the single-particle energy of the valence quark and the quark correlation in mesons. Such agreements may indicate the possible connection between the low energy quark model and the deep inelastic phenomena.

We thank Prof. Y. Mizuno for valuable discussions about the semi-inclusive electron nucleon scattering.

References

- [1] See e.g., R.G. Roberts, *The structure of the proton*, Cambridge Press (1990)
- [2] R.L. Jaffe and G.G. Ross, Phys. Lett. **B93** (1980) 313
- [3] C.J. Benesh and G.A. Miller, Phys. Rev. **D36** (1987) 1344
- [4] A.W. Schreiber, A.I. Signal and A.W. Thomas, Phys. Rev. **D44** (1991) 2653, and references therein.
- [5] L.S. Celenza and C.M. Shakin, Phys. Rev. **C27** (1983) 1561
C.J. Benesh and G.A. Miller, Phys. Lett. **B215** (1988) 381
R.P. Bickerstaff and T. Londergan, Phys. Rev. **D42** (1990) 3621
H. Meyer and P.J. Mulders, Nucl. Phys. **A528** (1991) 589
M.R. Bate and A.I. Signal, J. Phys. **G18** (1992) 1875
M. Tarini, L. Conci and U. Moschella, Nucl. Phys. **A544** (1992) 731
- [6] Y. Nambu and G. Jona-Lasinio, Phys. Rev. **122** (1961) 345, *ibid* **124** (1961) 246
- [7] M. Schaden, H. Reinhardt, P.A. Amundsen and M.J. Lavelle, Nucl. Phys. **B339** (1990) 595
- [8] U. Vogl and W. Weise, Prog. Part. Nucl. Phys. **27** (1991) 195
- [9] For a recent review, S.P. Klevansky, Rev. Mod. Phys. **64** (1992) 649
- [10] A. Ardekani and A.I. Signal, Phys. Lett. **B311** (1993) 281
- [11] T. Shigetani, K. Suzuki and H. Toki, Phys. Lett. **B308** (1993) 383
- [12] NA3 Coll., J. Badier *et al.*, Z. Phys. **C18** (1983) 281
NA10 Coll., B. Betev *et al.*, Z. Phys. **C28** (1985) 15
E537 Coll., E. Anassontzis *et al.*, Phys. Rev. **D38** (1988) 1377
E615 Coll., P. Bordalo *et al.*, Phys. Lett. **B193** (1987) 368
WA70 Coll., M. Bonesini *et al.*, Z. Phys. **C37** (1988) 535
W.J. Stirling and M.R. Whalley, J. Phys. **G19** (1993) D1, and references therein.

- [13] J. Badier *et al.*, Phys. Lett. **B93** (1980) 354
- [14] N.S. Craigie and G. Schierholz, Nucl. Phys. **B100** (1975) 125
- [15] M. Lusignoli and Y. Srivastava, Nucl. Phys. **B138** (1978) 151
M. Lusignoli and P. Pistilli, Nuovo Cim. Lett. **24** (1979) 81
M. Lusignoli, P. Pistilli, F. Rapuano, Nucl. Phys. **B155** (1979) 394
- [16] N. Yu. Volkonskii *et al.*, Sov. J. Nucl. Phys. **25** (1977) 79
- [17] V. Bernard, R.L. Jaffe and U.-G. Meissner, Nucl. Phys. **B308** (1988) 753
- [18] A. De Rújula and F. Martin, Phys. Rev. **D22** (1980) 1787
- [19] P. V. Landshoff, J. C. Polkinghorne and R. D. Short, Nucl. Phys. **B28** (1971) 225
- [20] V.L. Chernyak and A.R. Zhitnitsky, Phys. Rep. **112** (1984) 173
- [21] M. Glück, E. Reya and A. Vogt, Z. Phys. **C53** (1992) 651
- [22] G.E. Brown, M. Rho and W. Weise, Nucl. Phys. **A454** (1986) 669
- [23] G. Altarelli and G. Parisi, Nucl. Phys. **B126** (1977) 298
- [24] P.J. Sutton, A.D. Martin, R.G. Roberts and W.J. Stirling, Phys. Rev. **D45** (1992) 2349
- [25] C.L. Korpa and U.-G. Meissner, Phys. Rev. **D41** (1990) 1679
M. Burkardt and B.J. Warr, Phys. Rev. **D45** (1992) 958
- [26] P.V. Chliapnikov *et al.*, Nucl. Phys. **B148** (1979) 400
- [27] A. El Hassouni and O. Napoly, Phys. Rev. **D23** (1981) 193
- [28] Y. Nishino and T. Suzuki, to be published
- [29] K-W. Lai and R.L. Thews, Phys. Rev. Lett. **44** (1980) 1729
- [30] L. Mankiewicz, Phys. Rev. **D40** (1989) 255

- [31] M. Bishari, Phys. Lett. **B38** (1972) 510
- [32] New Muon Coll., P. Amaudruz *et al.*, Phys. Rev. Lett. **66** (1991) 2716
- [33] E.M. Henley and G.A. Miller, Phys. Lett. **B251** (1991) 453
- [34] S. Kumano, Phys. Rev. **D43** (1991) 3067
 S. Kumano and J.T. Londergan, Phys. Rev. **D44** (1991) 717
- [35] K. Suzuki, T. Shigetani and H. Toki, hep-ph/9310266, Nucl. Phys. **A** in press, and
 references therein.
- [36] T. Shigetani, H. Toki, K. Suzuki, in preparation
- [37] K. Suzuki and T. Shigetani, to be published

Table 1 Meson Properties

Parameters

$$m_{u,d} = 5.5MeV, m_s = 130MeV, \Lambda = 900MeV,$$

$$G_S\Lambda^2 = 2G_V\Lambda^2 = 19, a = 0.15GeV^2$$

	Theoretical values	Empirical values
Pion mass	140MeV	140MeV
f_π	93MeV	93MeV
Kaon mass	498MeV	495MeV
f_K	96MeV	114MeV
M_u	370MeV	
M_s	548MeV	
$\langle \bar{\psi}\psi \rangle$	$(-250MeV)^3$	$\sim (-250MeV)^3$
$g_{\pi qq}$	3.92	

Figure Captions

Fig. 1 (a) : The Dyson equation for the quark propagator. The thick solid line represents the dressed constituent quark, and the thin solid line the current quark.

Fig. 1 (b) : The Bethe-Salpeter equation for quark-antiquark scattering. \mathcal{T} is the quark-antiquark T-matrix with the total momentum q . \mathcal{K} denotes the interaction kernel discussed in the text.

Fig. 2 : The forward scattering amplitude ("handbag diagram") of the pion. The solid line represents the quark, and dashed line the meson. The virtual photon is depicted by the wavy line. For details and notation, see text.

Fig. 3 : The quark distributions of the pion at the low energy model scale $Q^2 = Q_o^2$ as a function of the Bjorken x .

Fig. 4 : The quark distributions of the kaon at the low energy model scale $Q^2 = Q_o^2$. The u-quark distribution is depicted by the solid curve, and the s-quark distribution by the dashed curve.

Fig. 5 : The valence quark distribution of the pion at $Q^2 = 20GeV^2$ (solid curve) as a function of the Bjorken x , in which we use the model scale $Q_o^2 = 0.25GeV^2$. The experimental fit[24] is depicted by the dashed curve.

Fig. 6 : The valence quark distribution of the pion at $Q^2 = 20GeV^2$ with the model scale $Q_o^2 = 0.7GeV^2$. The notations are the same as those in Fig.5.

Fig. 7 : The pion structure function at $Q^2 = 20GeV^2$. The experimental data are taken from the NA3 experiment[12]. The theoretical prediction of the NJL model is depicted by the solid curve. Here, we use $F_\pi(x) = Kxq(x)$ with the sea quark distributions being neglected, where we take the K -factor, $K = 1.5$ [24].

Fig. 8 : The valence quark distributions in the kaon at $Q^2 = 20\text{GeV}^2$ with the model scale $Q_0^2 = 0.25\text{GeV}^2$. The u-quark distribution is depicted by the solid curve, and the s-quark distribution by the dashed curve.

Fig. 9 : The ratio of kaon to pion valence u-quark distributions $u_K(x)/u_\pi(x)$ at $Q^2 = 20\text{GeV}^2$. The theoretical result is depicted by the solid curve. The closed circles with error bars are taken from the Drell-Yan experiment[13]. The open circle line with the dotted area, which indicates the error, is obtained by taking a ratio of the parameterization in ref. [29], where the pion and kaon structure functions are determined by the data on the large transverse momentum π_0 productions. For comparison, the results with $M_s/M_u = 2$ and 1 are shown by the dashed and dotted curves, respectively.

Fig. 10 : The valence quark distribution in the rho meson at the model scale as a function of the Bjorken x .

Fig. 11 : The semi-inclusive lepton nucleon scattering. The solid line represents the electron and the doubled line the nucleon. The virtual pion and the virtual photon are depicted by the dashed and wavy lines.

Fig. 12 : The off-shell dependence of the quark distribution in the pion. The results at $t = m_\pi^2$ (on-shell), and $t = -0.1, -0.25, -0.5\text{GeV}^2$ are shown.

Fig. 13 : $d\sigma/dp(e + p \rightarrow e' + n + X)$ as a function of p with $E_L = 30\text{GeV}$. In Fig.13 (a), the triple Regge formula is used for the πNN vertex, and the dipole cutoff in Fig.13 (b). The theoretical result is depicted by the solid curve. The results using the distribution of Sutton *et al.*[24] and Glück *et al.*[21] are also shown by the dashed and dotted curves, respectively.

Fig. 14 : $d\sigma/dx(e + p \rightarrow e' + n + X)$ as a function of the Bjorken x with $E_L = 30\text{GeV}$. The triple Regge formula is utilized in Fig. 14 (a), whereas the dipole formula in Fig.14 (b). The notations are the same as those in Fig.13. The result in terms of the calculated

structure function with no off-shell dependence is also shown by the dash-dotted curve.

Fig. 15(a) : The lowest order sea quark diagram in the NJL model. The solid line denotes the quark, and the wavy line the virtual photon.

Fig. 15(b) : The next to leading order sea quark diagram in the NJL model. The dashed line indicates the pion.

This figure "fig1-1.png" is available in "png" format from:

<http://arXiv.org/ps/hep-ph/9402277v1>

This figure "fig2-1.png" is available in "png" format from:

<http://arXiv.org/ps/hep-ph/9402277v1>

Fig. 1 (a)

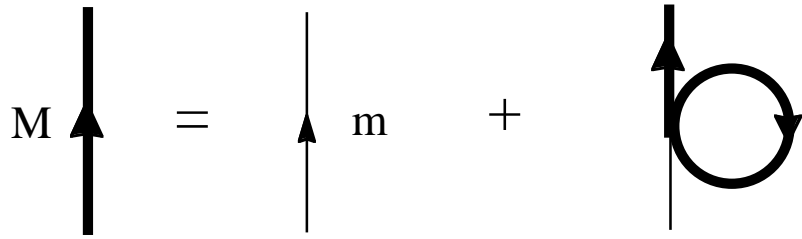


Fig. 1 (b)

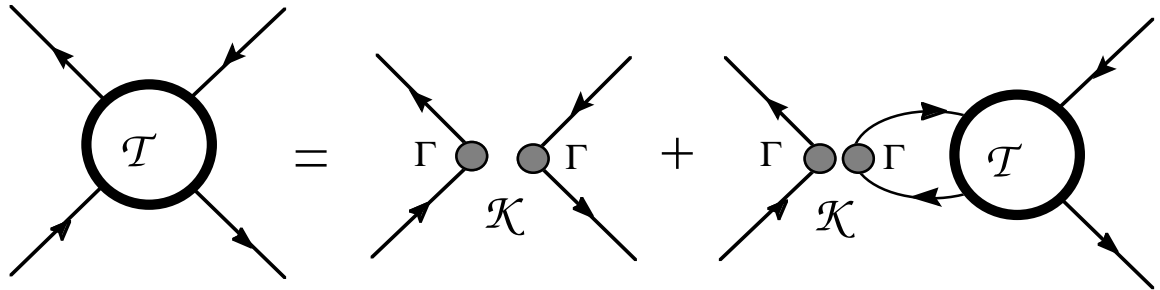
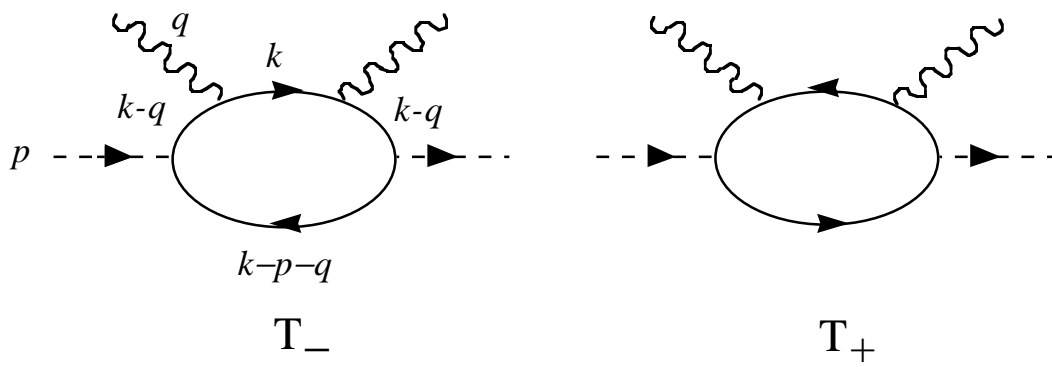


Fig. 2



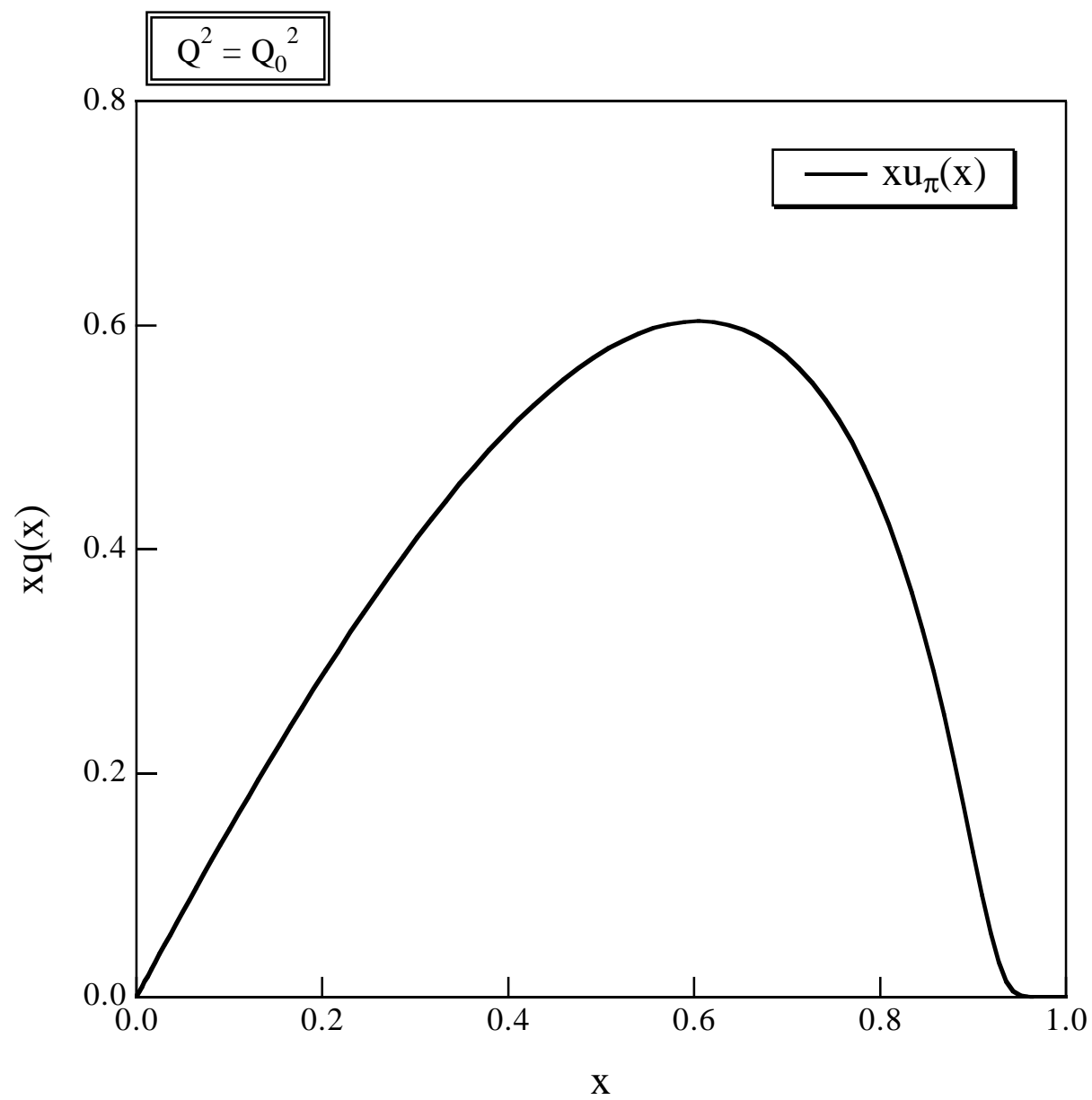
This figure "fig1-2.png" is available in "png" format from:

<http://arXiv.org/ps/hep-ph/9402277v1>

This figure "fig2-2.png" is available in "png" format from:

<http://arXiv.org/ps/hep-ph/9402277v1>

Fig. 3



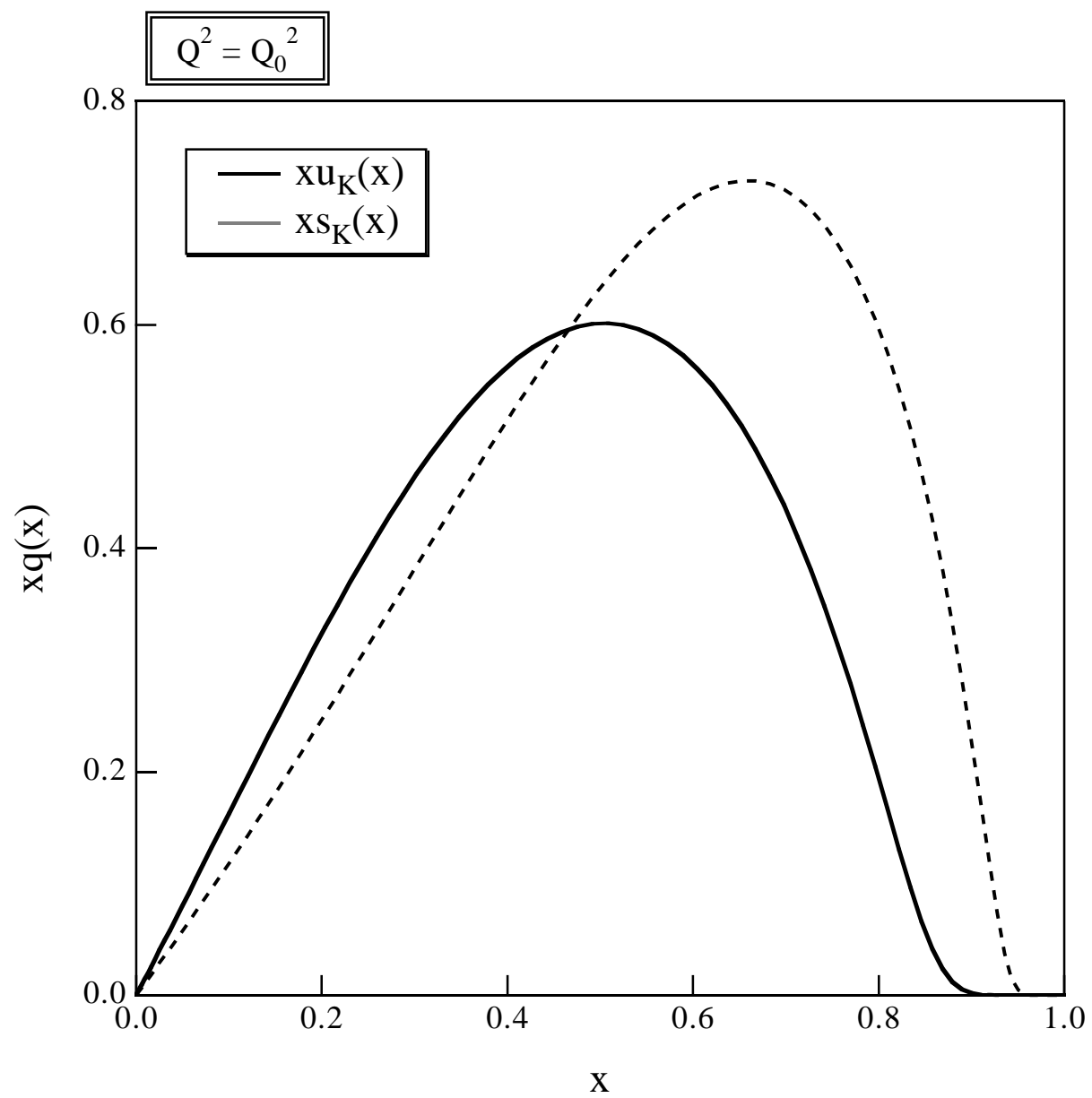
This figure "fig1-3.png" is available in "png" format from:

<http://arXiv.org/ps/hep-ph/9402277v1>

This figure "fig2-3.png" is available in "png" format from:

<http://arXiv.org/ps/hep-ph/9402277v1>

Fig. 4



This figure "fig1-4.png" is available in "png" format from:

<http://arXiv.org/ps/hep-ph/9402277v1>

This figure "fig2-4.png" is available in "png" format from:

<http://arXiv.org/ps/hep-ph/9402277v1>

Fig. 5

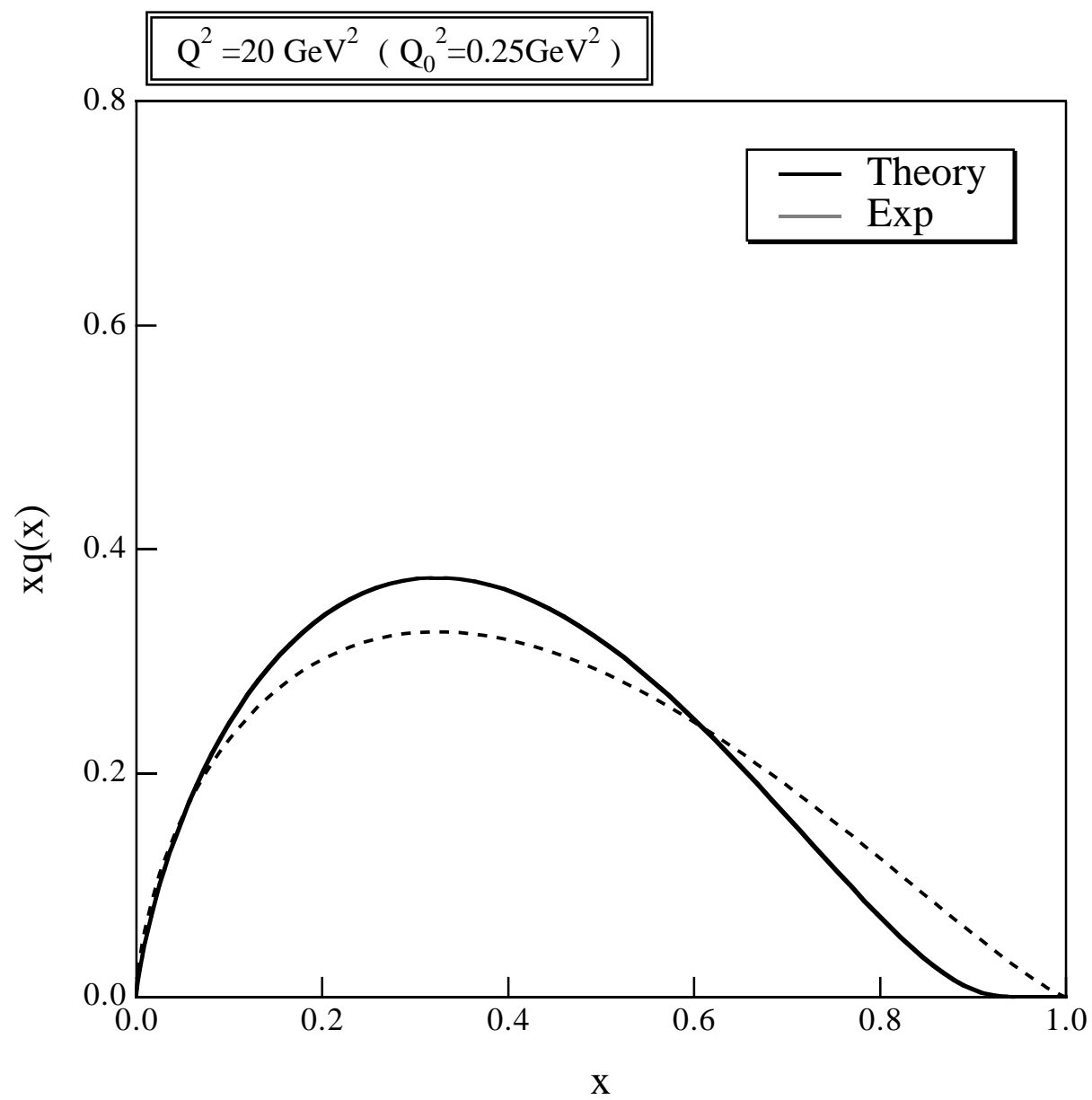


Fig. 6

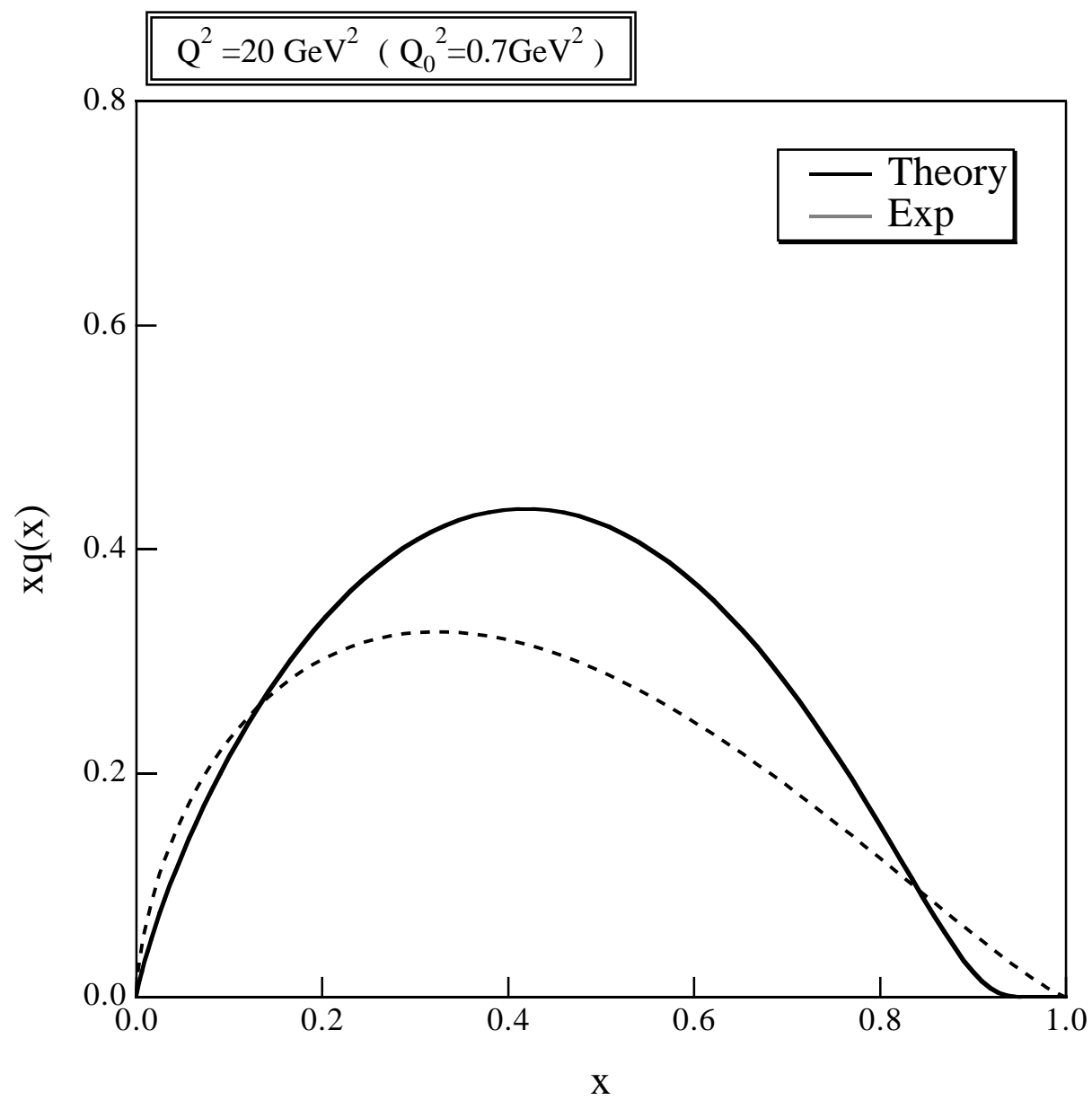


Fig. 7

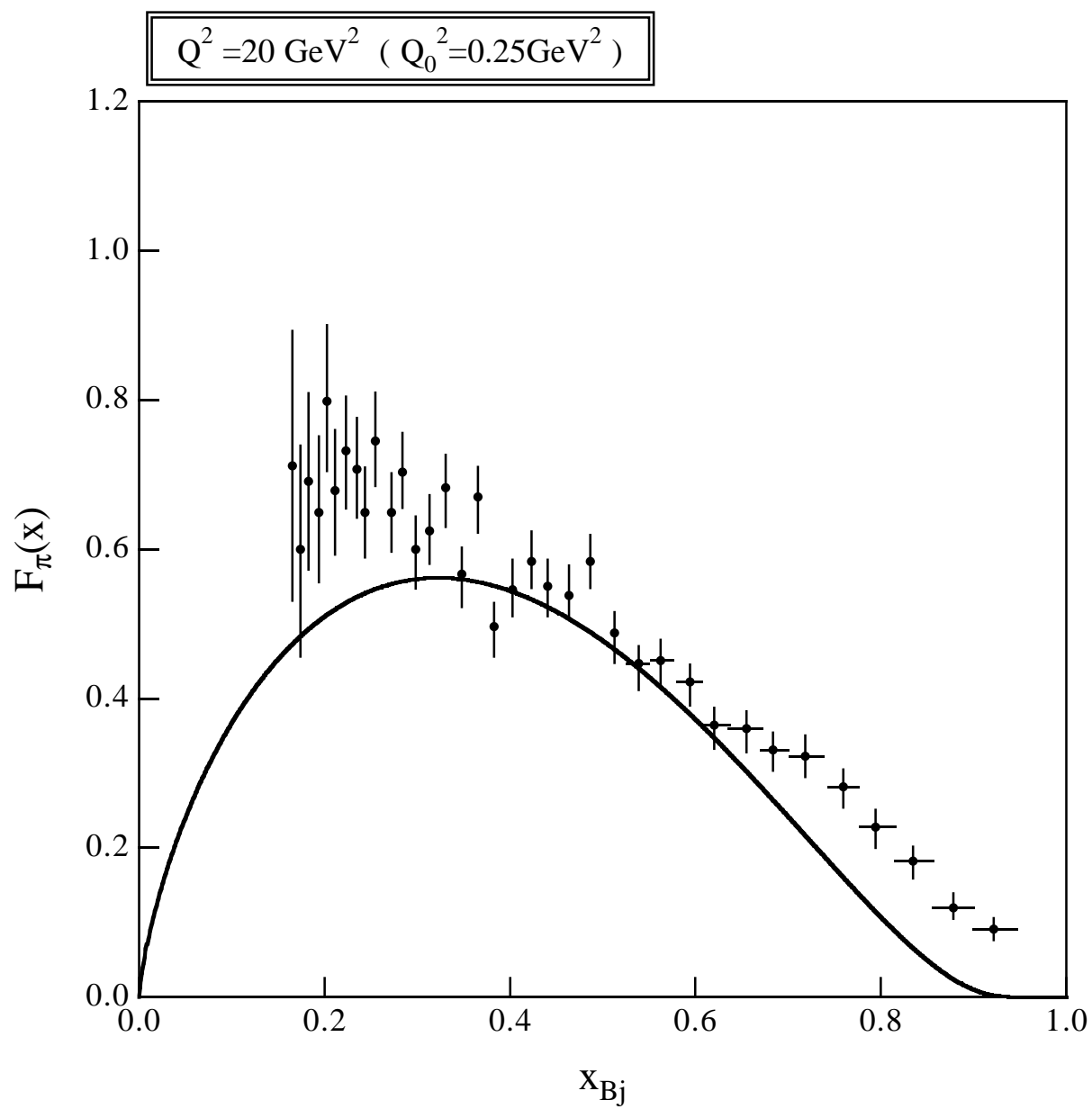


Fig. 8

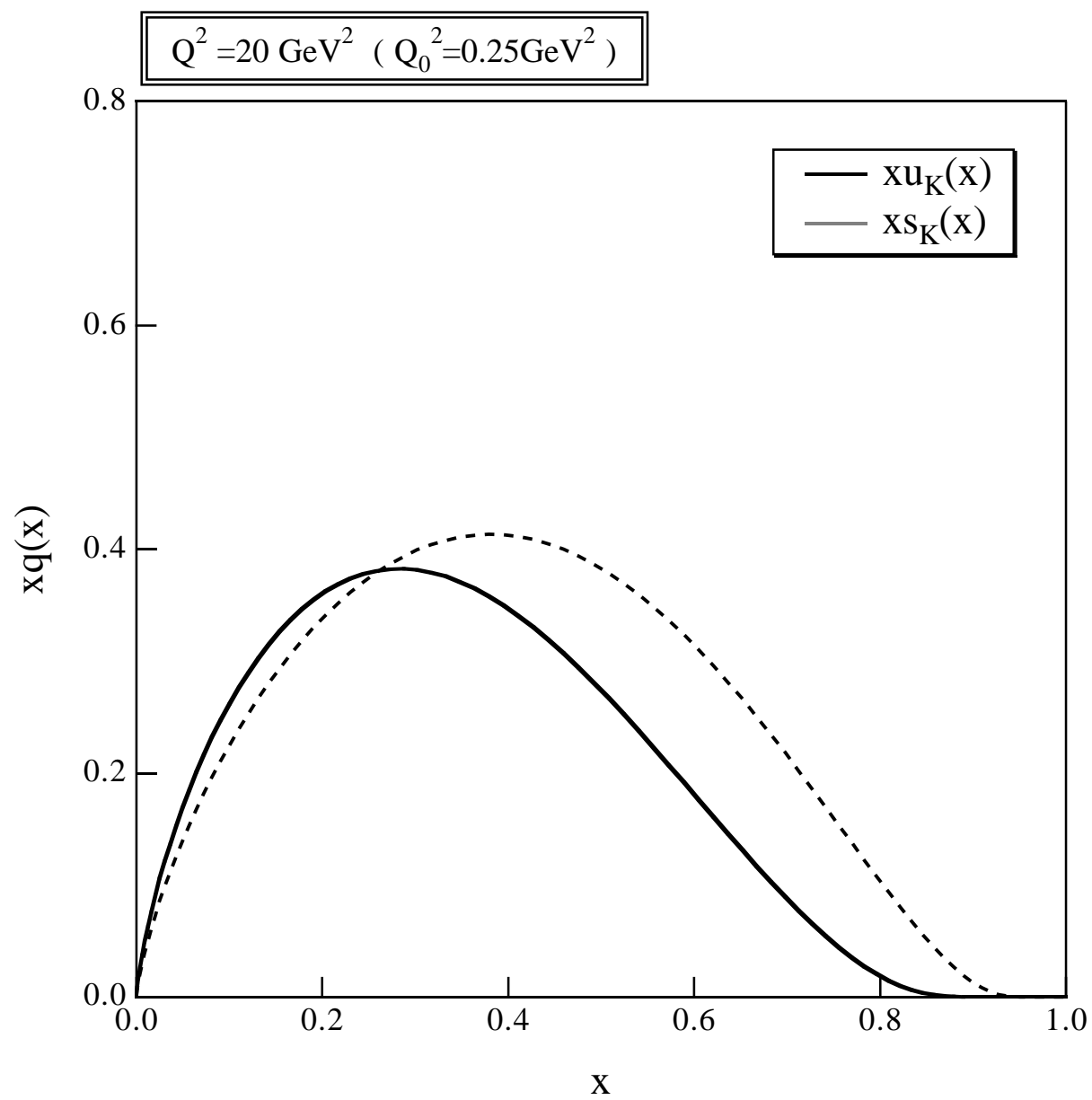


Fig. 9

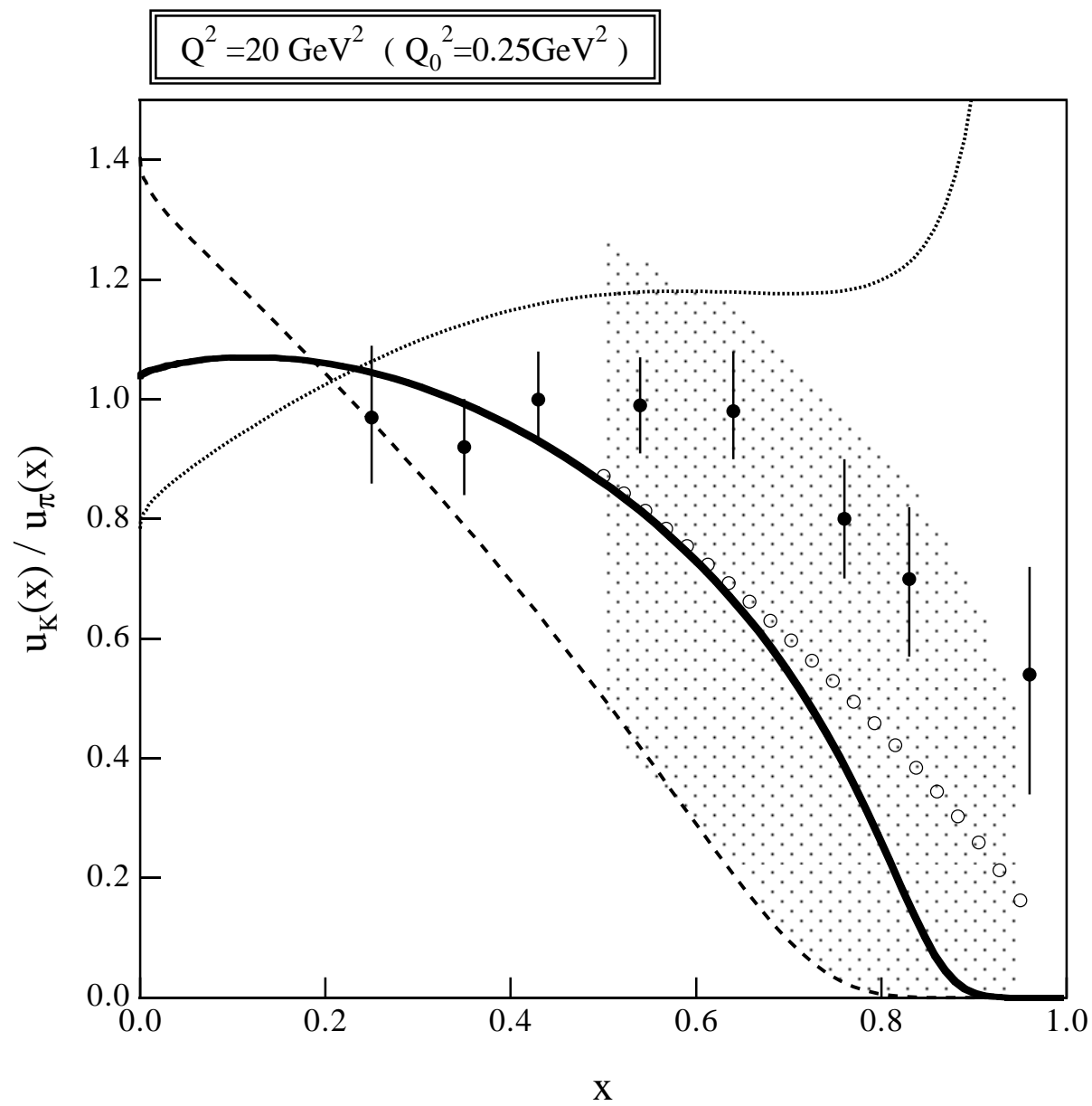


Fig. 10

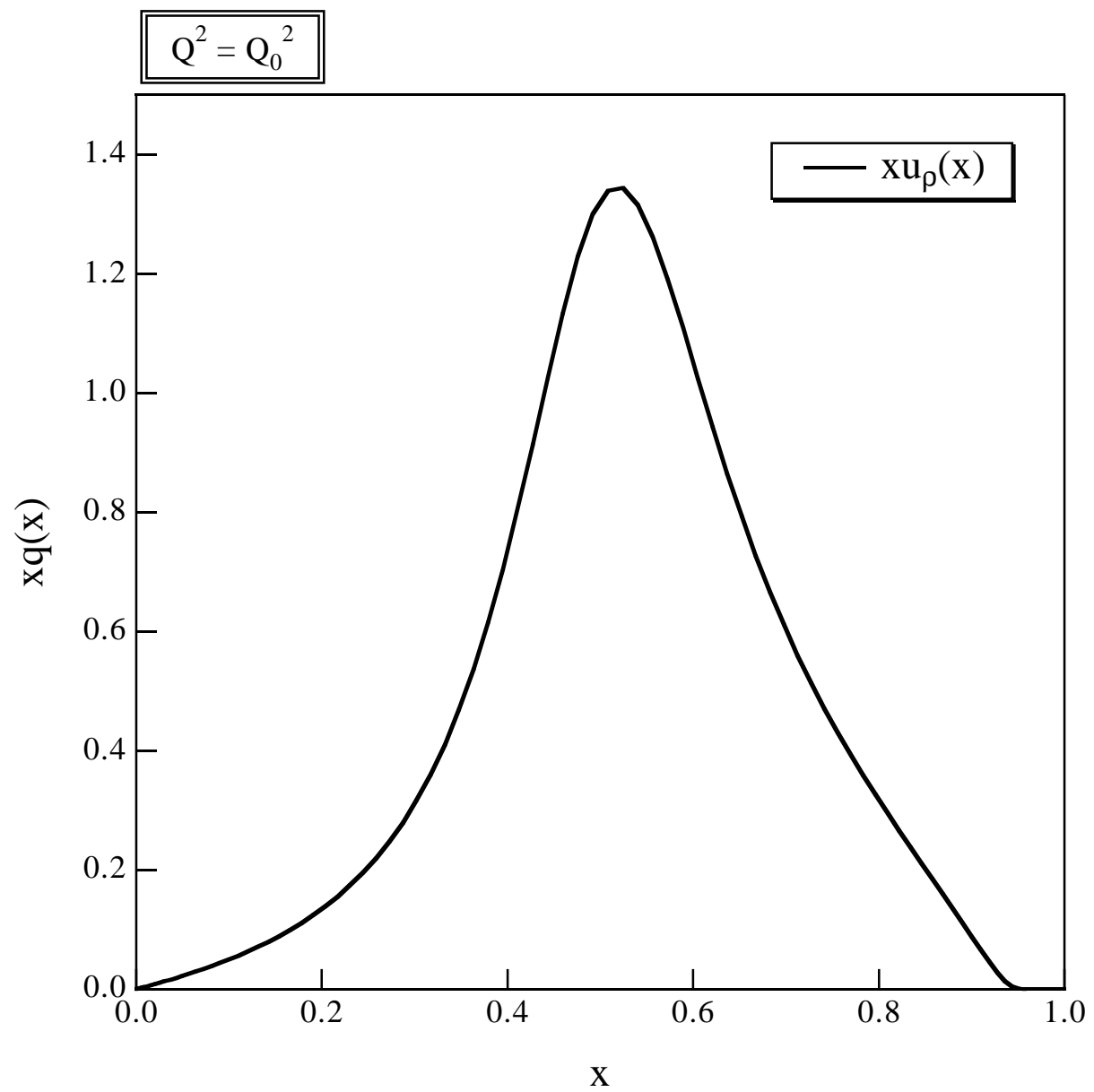


Fig.11

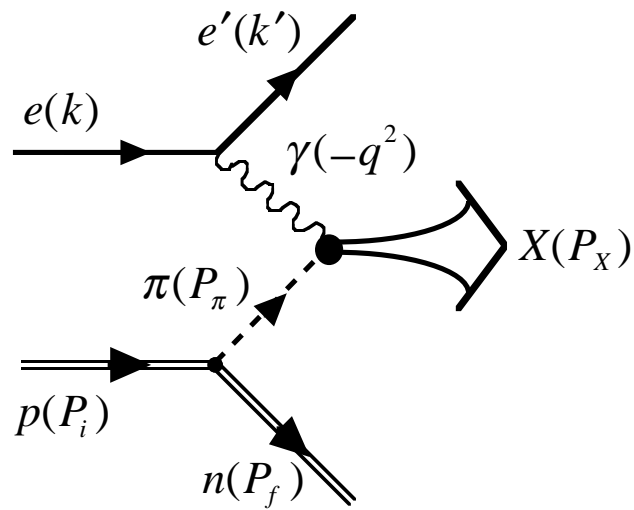


Fig.12

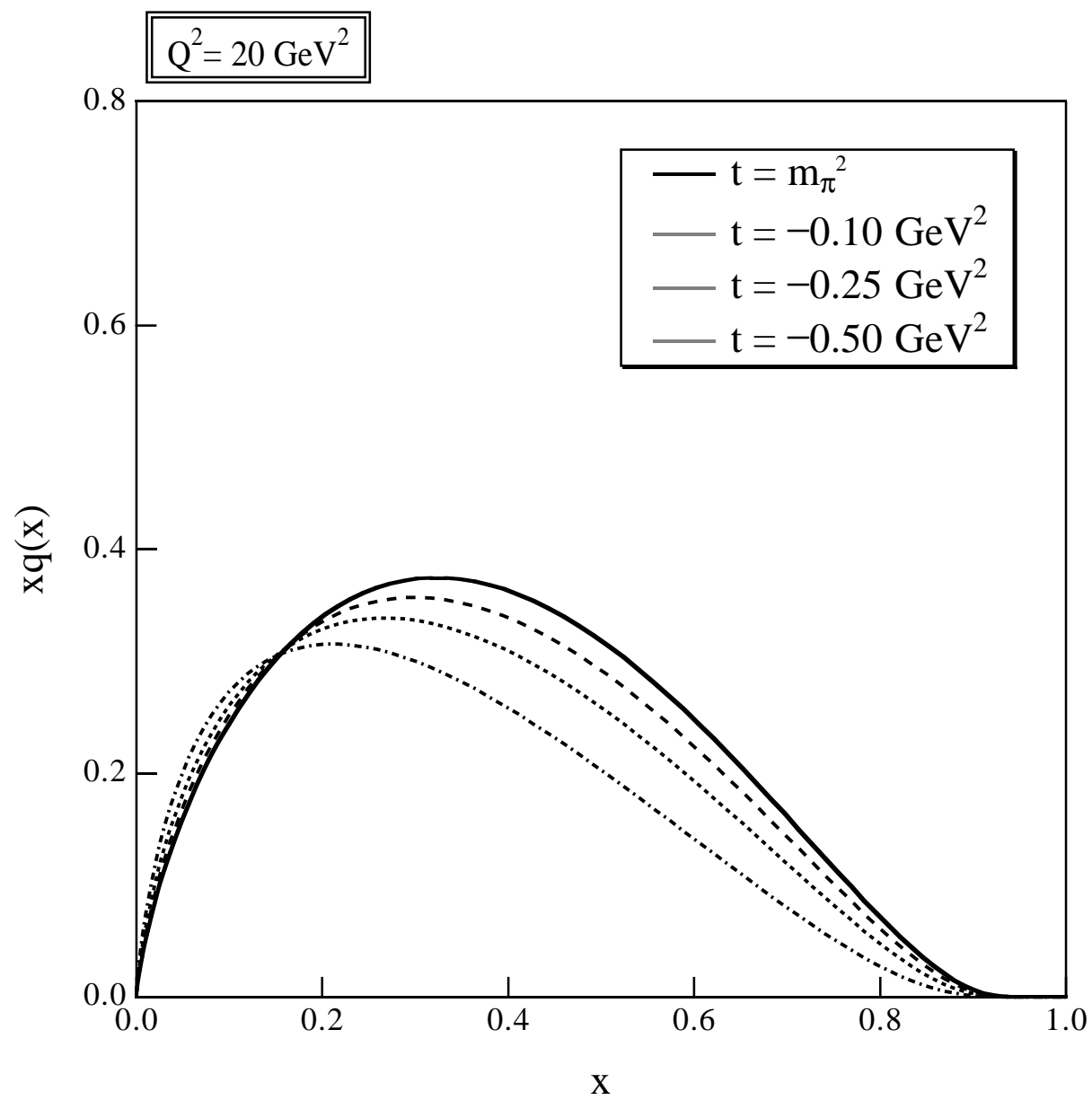


Fig.13(a)

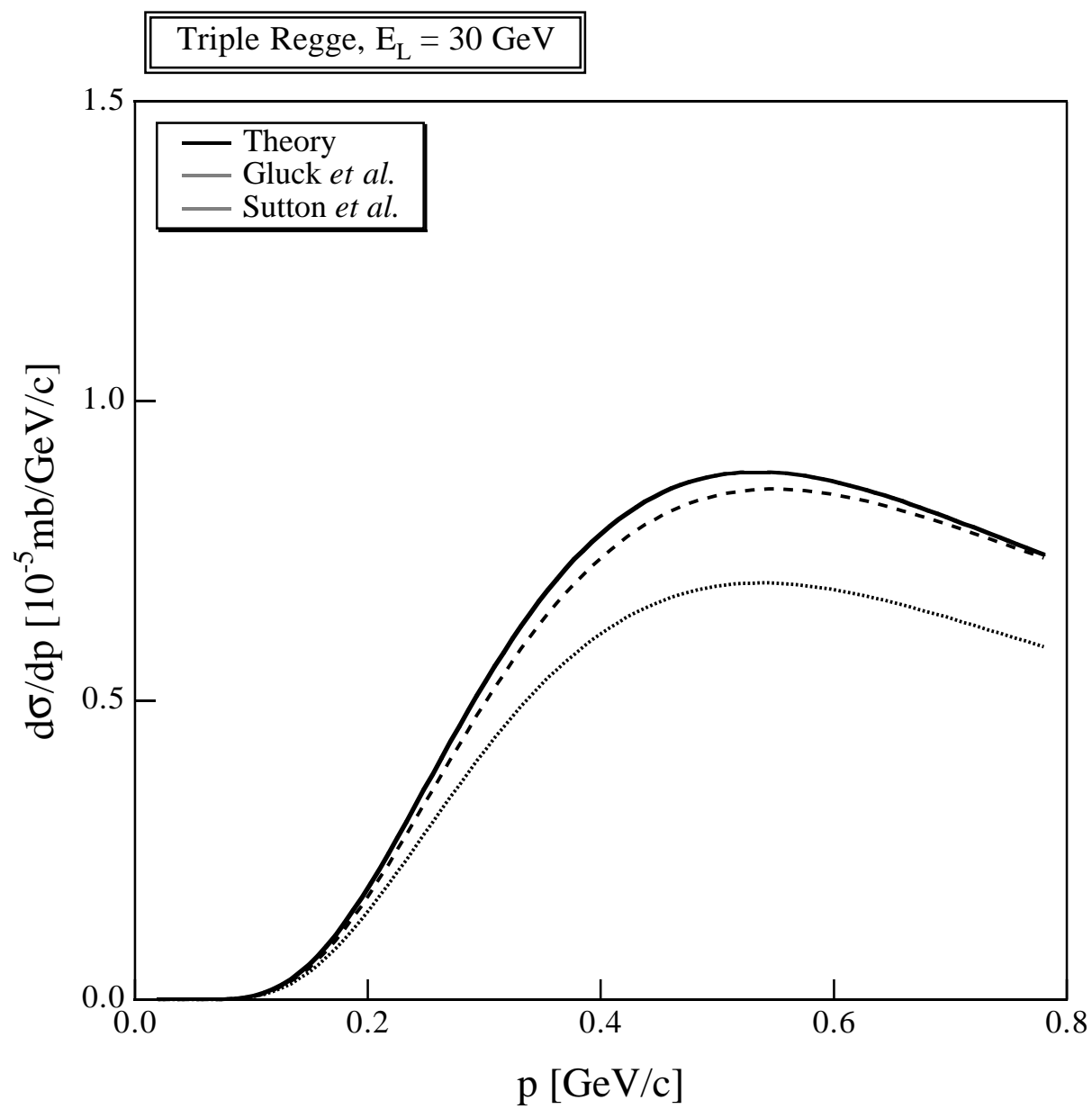


Fig.13(b)

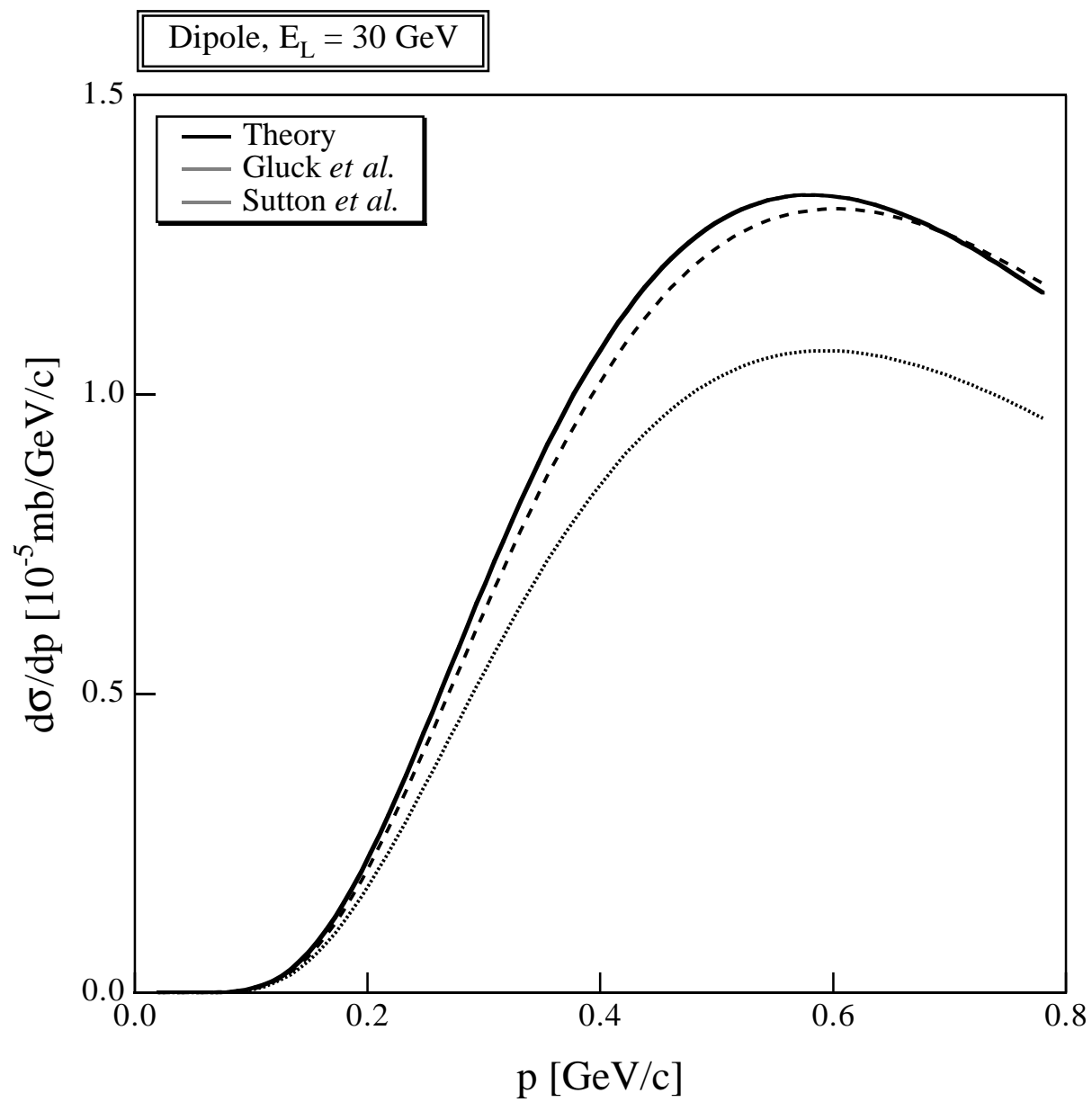


Fig.14(a)

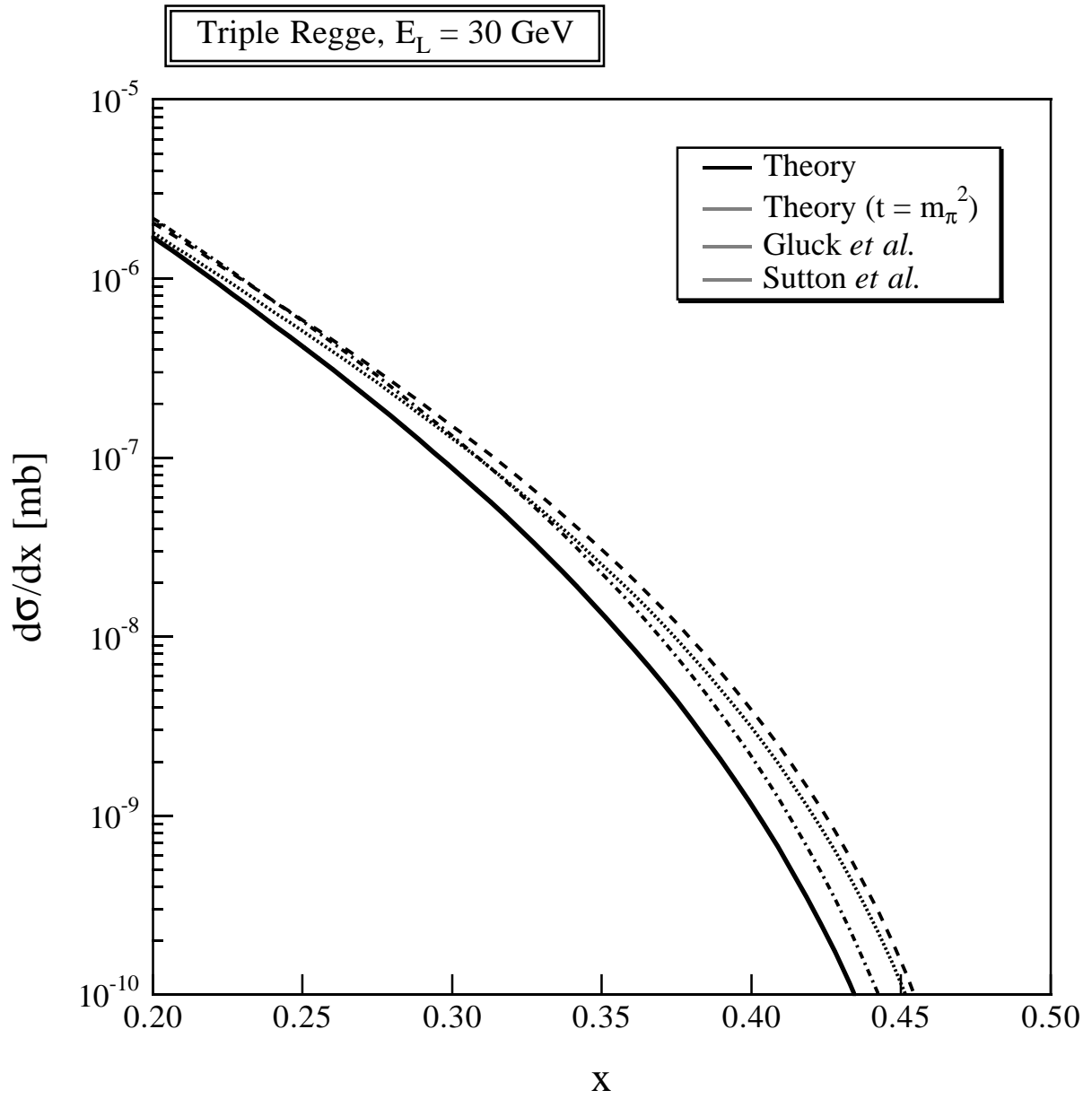


Fig.14(b)

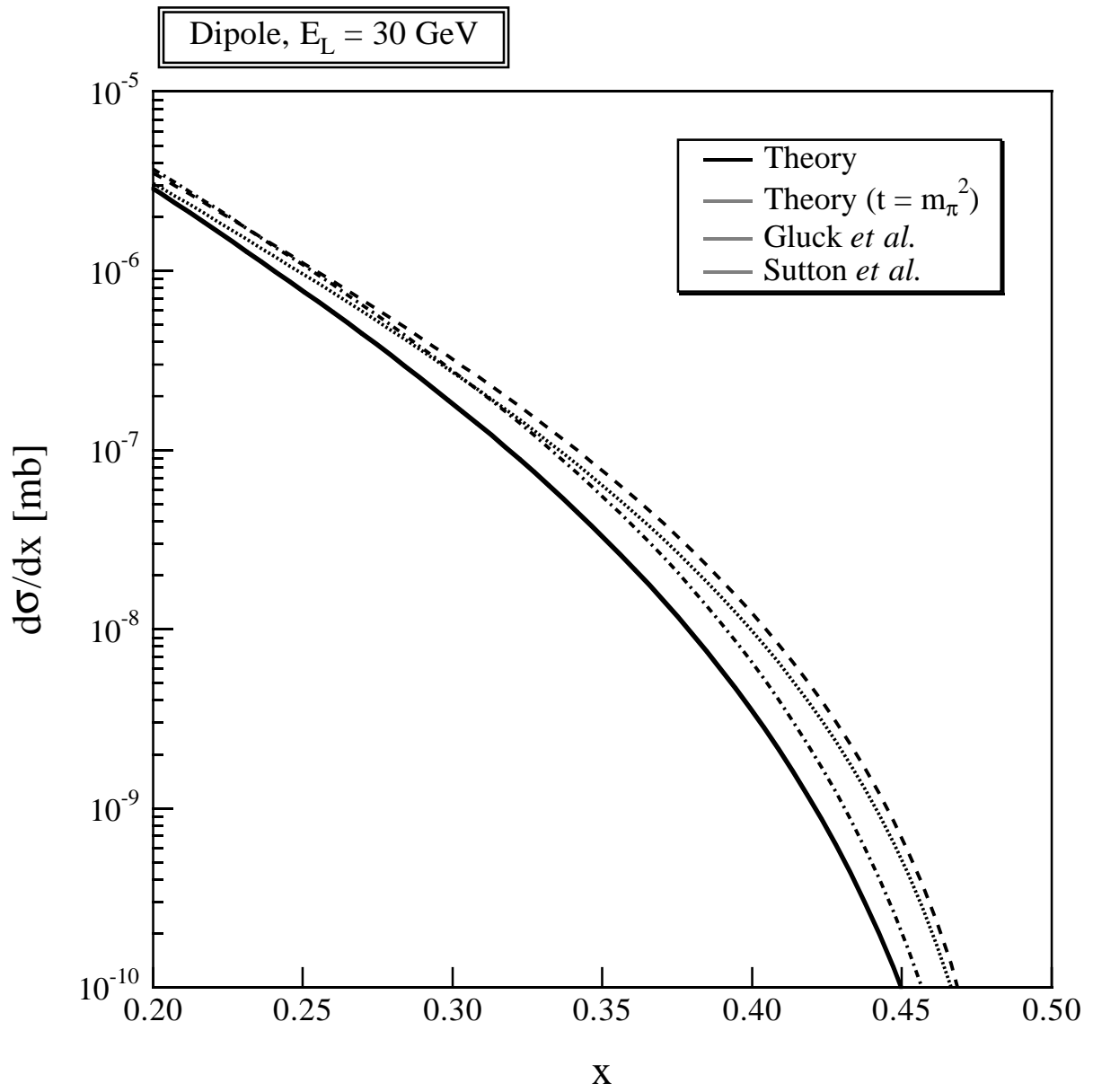


Fig. 15(a)

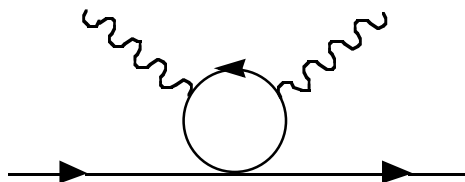


Fig. 15(b)

